A98-25240 AIAA-98-1990

OPTIMIZATION OF PANELS WITH RIVETED Z-SHAPED STIFFENERS VIA PANDA2

David Bushnell Dept. H1-61, Bldg. 250
Lockheed Martin Advanced Technology Center
3251 Hanover St., Palo Alto, California 94304

ABSTRACT

The PANDA2 computer program has been modified to permit minimum weight design of imperfect panels with riveted Z-shaped stiffeners for service in a load regime in which the panel is in its locally postbuckled state. Perfect and imperfect panels optimized with PANDA2 are evaluated via nonlinear STAGS analyses. The agreement between predictions by PANDA2 and STAGS is sufficient to qualify PANDA2 as a preliminary design tool for panels with riveted Z-shaped stringers. Optimum designs for panels with Z-shaped stringers are compared to those with J-shaped and T-shaped stringers.

INTRODUCTION

In the late 1970's van der Neut [1] obtained approximate buckling load factors for the overall buckling of uniformly axially compressed flat panels with either bonded or riveted Z-shaped stringers. He checked his results by comparing with predictions from the VIPASA code by Wittrick and Williams [2,3].

Riks [4] performed an analysis with use of the STAGSC1 program [5]. He included a study of sensitivity of the load factor corresponding to overall buckling to initial bowing imperfections, finding unstable postbuckling behavior (imperfection sensitivity) caused by deformation of the stringer cross section in the overall buckling mode. In "classical" wide column buckling of a panel stiffened with T-shaped stringers, for example, the T-stringer cross section remains undeformed as it translates normal to the skin surface in the wide column buckling mode. This is not so with Z-stiffened panels. In that case, because the stringers have a nonsymmetric cross section, they undergo significant sidesway as the panel skin essentially translates normal to the undeformed panel skin in the overall buckling mode (see Fig. 11, for example). Hence, the load at which a Z-stiffened panel collapses under uniform axial compression is sensitive to an initial overall bowing imperfection even if the local buckling load factor significantly exceeds that corresponding to general ("wide column") instability.

Local and overall bifurcation buckling of panels with Z-shaped stringers can also be determined with the BUCLASP code [6] and with the newer successors to BUCLASP and VIPASA: the PANDA2 [7], POSTOP [8], VICONOPT [9], and PASCO [10] codes. PASCO, VICONOPT, PANDA2 and POSTOP are capable of obtaining optimum designs of such panels and PANDA2 and POSTOP can do so including the effect of local postbuckling [11] of the panel skin and/or parts of the stringers. The authors of VICONOPT [9] are currently working on a postbuckling capability [9]. One of the PANDA2 processors, called STAGSMODEL [12] automatically sets up a finite element model of a panel previously optimized with PANDA2. The PANDA2/STAGSMODEL/STAGS combination has been used many times to optimize and evaluate optimum designs of panels under combined loads for service in the postbuckling regime [11-15].

Other significant contributions to the field of buckling and postbuckling of panels include works by Stein [16], Leissa [17], Arnold and Parekh [18], Starnes, Knight, and Rouse [19], Spier [20,21], Khot and Bauld [22,23], Zhang and Matthews [24], Gürdal and his colleagues [25-31], Haftka and his colleagues [30-36, 61], Librescu and his colleagues [37-39], Sridharan and his colleagues [40,41], Knight and his colleagues [42-44], Myers and Hyer [45], Nemeth [46], Noor, Starnes, and Peters [47], and McGowan and Anderson [48] and Wiggenraad, et al [62].

Fellow, AIAA

METHOD OF ANALYSIS

In PANDA2 local buckling of a stringer-stiffened panel is predicted from a single-module discretized model described in [7]. (See Fig. 22(a,b) in [7] and Fig. 8 in this paper, for examples). Overall buckling is predicted from both a single-module discretized "wide column" model, such as shown in Fig. 22c of [7] and Fig. 9 of this paper, and from a model in which the stiffeners are "smeared out" (averaged) over the panel in the manner of Baruch and Singer [49]. Discretization is via the finite difference energy method, as described in [50]. There are a number of nodal points in each of the segments of the module cross section, and variation along the axis of the panel is assumed to be trigonometric with the critical number of axial halfwaves and critical slope of buckling nodal lines in the panel skin (for an anisotropic panel and/or a panel in which in-plane shear loading Nxy is present) determined in the analysis described in detail in [11].

The purpose of the work reported here is to enhance the capability of PANDA2 by inclusion of Z-shaped stiffeners riveted to the panel skin. A discretized panel skin-stringer single module is constructed as shown in Fig. 1. The stringer spacing is called "b" and the rivet line, considered to be continuous in the axial direction and located at the midwidth of the attached flange (Segment 2 of the single module), is located at b/2, the midwidth of the entire module. The toe and heel of the attached flange are free to separate from or to "penetrate" the panel skin in the local buckling mode and in the post-local buckling regime: no intermittant contact conditions are imposed in the PANDA2 model. At the rivet line compatibility conditions are imposed between panel skin and attached flange with eccentricity of the attached flange with respect to the reference surface of the panel skin accounted for.

Local buckling modes typically have a form such as shown in Fig. 8, which is assumed to be sinusoidal in the axial direction with a computed critical number of axial halfwaves and a computed slope of the local buckling nodal lines [11,22,23] in the critical local buckling mode. The local buckling nodal lines are assumed to be straight. The nonlinear local postbuckling analysis [11] is analogous to that of Koiter [51]. In PANDA2 the axial wavelength and the slope of the nodal lines of the postbuckled pattern are permitted to change as the applied load is increased above that corresponding to initial local bifurcation buckling. Details of the nonlinear post-local buckling analysis and predictions from PANDA2 and STAGS [52] appear in [11].

The "wide column" buckling mode has a form such as shown in Fig. 9. There is assumed to be one-half wave in the axial direction in the "wide column" mode. The "softening" effect which influences the effective overall axial, hoop, and in-plane shear membrane stiffness components of a locally imperfect and/or locally postbuckled panel module (See Fig. 15 of [12], for example) is accounted for in the computation of the bending-torsional, "wide column" and overall buckling load factors.

IMPLEMENTATION OF Z-SHAPED STRINGERS INTO PANDA2

The file that contains prompting phrases and "help" paragraphs for the user was modified to include Z-shaped stiffeners. Special sketches for Z-shaped modules were introduced into the PANDA2 input prompts and output as depicted in Figs. 1 (a,b).

In order to maintain conservativeness of optimized designs, no allowance is made in PANDA2 for clamping Z-shaped stringer stiffened panels along the two axially loaded ends as opposed to simple support there. In the computation of "effective" axial length (described for clamped panels in [7] and in ITEMS 3, 79a, 105e, 106, and 113d,r of the PANDA2 documentation file, ...panda2/doc/panda2.news [53]), a panel with Z-shaped stringers is ALWAYS treated as if it were simply supported along its two axially loaded ends even if the user indicates clamping there. This strategy was introduced during the testing phase of implementation of the "Z" capability. Comparison of results from PANDA2 and STAGS [52] revealed that this strategy is required to maintain conservativeness of optimum designs of imperfect (bowed) panels generated by PANDA2.

It is thought that this new strategy, now introduced into PANDA2 also for J-shaped stringer stiffened panels, compensates for the softening effect on effective axial stiffness of sidesway of the "unbalanced" stringers as an initially axially bowed panel with Z or J stringers deforms further under application of axial compression [4]. (By "unbalanced" is meant here a stringer which is not symmetrical with respect to a plane normal to the panel skin and containing the line of attachment of the

stringer to the panel skin). Unfortunately, in its nonlinear Koiter-type postbuckling analysis [11], PANDA2 accounts for deformation of the single module cross section ONLY in the LOCAL buckling mode, not also in the "wide column" (general) buckling mode. (Note, however, that in one of the branches in which the maximum stresses are computed, PANDA2 does include this effect in an approximate manner, as described in [54]).

It is emphasized here that the neglect of further stiffener sidesway in PANDA2's analysis of the overall collapse of Z or J stiffened panels with overall initial buckling modal imperfections may well lead to the generation of unconservative designs in the case of imperfect Z or J stiffened panels that are actually simply supported along the two axially loaded ends. In such cases, the user should introduce factors of safety for inter-ring and overall buckling that are greater than unity, perhaps in the range 1.2 - 1.5.

The sequence of execution of PANDA2 modules called BEGIN, DECIDE, MAINSETUP, PANDAOPT, CHOOSEPLOT, DIPLOT, etc. is described in [7] and [53]; the use of the processor called SUPEROPT (for obtaining global optimum designs) is discussed in [14]; and the "automatic" generation of STAGS finite element models of panels previously optimized by PANDA2 via the PANDA2 processor called STAGSMODEL is demonstrated in [12]. There also exists a PANDA2 processor called PANEL [7] that generates an input file for BOSOR4 [50] for a panel previously optimized by PANDA2. (PANEL is valid only for panels with insignificant in-plane shear loading). The BOSOR4 model of the panel generated by PANEL is of "annular" form, as described in [55].

Optimization in PANDA2 is performed via the ADS routines written by Vanderplaats and his colleagues [56,57].

There are five types of analysis that can be performed by the PANDA2 mainprocessor, PANDAOPT. These types of analysis are controlled by an index called ITYPE as follows:

ITYPE=1 means an optimization analysis will be performed.

ITYPE=2 means PANDA2 will perform a buckling/stress analysis of a fixed design.

ITYPE=3 means PANDA2 will simulate a test of a panel with fixed design: For one of the load sets the behavior of the panel under monotonically increasing loads will be investigated.

ITYPE=4 means that margins will be calculated for all design variables fixed except one user-selected variable. Margins will be calculated for a sequence of designs in which the user-selected variable is incremented from a user-selected starting value to a user-selected ending value.

ITYPE=5 means that margins and interaction curves will be calculated for a user-selected in-plane load combination: (N1,N2) = (Nx,Ny) or (Nx,Nxy) or (Ny,Nxy)

SUMMARY OF NUMERICAL RESULTS

Optimization is performed for flat aluminum, elastic panels with Z-shaped, J-shaped, and T-shaped stringers. There are no transverse stiffeners (no rings). The panels are subjected to uniform axial compression, Nx = -2000 lb/in, and are clamped along the two axially loaded edges. All properties and decision variables and their lower and upper bounds are listed in Table 1. A typical PANDA2 runstream for optimization is listed in Table 2. Results for this study are summarized in Tables 3 and 4. Full details appear in [58].

Results from ten cases are summarized in Table 3 (columns 1 - 10 in Table 3): eight of the cases for a panel with riveted Z-shaped stringers, one for a panel with bonded J-shaped stringers and one for a panel with bonded T-shaped stringers. The first five cases (columns 1 - 5 in Table 3) are for perfect panels and the second five cases (columns 6 - 10) are for panels with an initial general buckling modal imperfection with amplitude equal to plus or minus 0.1 in. The first three cases (columns 1 - 3) are for a perfect panel in which local postbuckling is NOT permitted. In the first two cases the stringer spacing b is held constant at 10.0 inches, and in the remaining 8 cases the stringer spacing is one of the decision variables. The effect of the "modejump constraint" (See [15]) is explored for a perfect panel in Cases 4 and 5 and for an imperfect panel in Cases 6 and 7. For the optimum designs obtained by PANDA2 comparisons are made with predictions from BOSOR4 [50] and STAGS [52]. The units used in this study are inches and lbs.

Table 4 lists comparisons from PANDA2 and STAGS

for the maximum effective stresses in the optimized designs corresponding to Cases 4, 5, 6, 7, 9, and 10. In all these cases the axial load, Nx = -2000 lb/in, corresponds to the panel being loaded well beyond local buckling. (See PART 3 of Table 3).

Design margins corresponding to the optimum design for each of the 10 cases are listed in PART 12 of Table 3. In PANDA2 buckling margins are defined as follows:

buckling margin =

(buckling load factor)/(factor of safety) -1.

Although in this case the PANDA2 user (the writer) assigned the value 1.0 to all factors of safety (see Table 8 of [58]), PANDA2 automatically changes the factors of safety for local buckling and general buckling to 1.1 if the user-provided value is close to unity and less than 1.1. This is done in order to avoid the almost singular behavior that usually occurs in the neighborhoods of buckling loads, such as the very steep growth with increasing load of the amplitude of the local postbuckling normal displacement in the neighborhood of the local bifurcation buckling load (see Fig. 6 on p. 48 of [11]) and such as the very steep growth of an imperfection in the form of the general instability buckling mode that occurs in the neighborhood of the general instability buckling load [54]. These adjustments of the factors of safety for local and general buckling have the effect of "smoothing" the behavior of the buckling and stress constraint conditions from design iteration to iteration during an optimization process because very large bending stress gradients with respect to perturbations of the decision variables are avoided. PANDA2 automatically assigns factors of safety (denoted FS in PART 7 of Table 9 of [58]) for certain types of buckling, such as FS=1.4 for buckling of stringer segments 3 and 4 together, FS = 1.6 for rolling only of stringers, and FS = 1.2 for "hiwave" rolling of stringers. These factors of safety were established based on comparisons between results from PANDA2 and BOSOR4 and between results from PANDA2 and STAGS made over the years during which PANDA2 has been under continuous development [53].

Stress margins in PANDA2 are defined as follows:

stress margin =

(allowable stress)/[(actual stress)(factor of safety)] -1.

RESULTS FOR b = 10.0 in.: NON-OPTIMIZED **PERFECT** PANEL

These results correspond to the initial design listed in Table 1. Figures 2 and 3 pertain to this section. The initial thickness of the attached flange (t2 in Table 1) was intentionally set small so that there would be significant deformation in the attached flange in the local buckling mode.

From a PANDA-type (closed form) analysis [7,59] a critical local buckling load factor of 0.913 is predicted corresponding to 5 axial halfwaves. As described in [7,59], the "PANDA-type" model of local buckling of the panel skin is based on the assumption that the segment of panel skin between adjacent stringers (the "local" plate) is simply supported along all four edges. In this case the length of the "local" plate is 50 inches and the width of the "local" plate is equal to the stringer spacing, b = 10 inches (Table 1). The local buckling load factor from the discretized single module model is much less than 0.913; it is 0.516, as shown in Fig. 2.

Why is the "classical" simply-supported "local" plate model so unconservative in this case? Figure 2 demonstrates. The critical "local" buckling mode from the single discretized module model in this case is not of the "classical" type shown in Fig. 8, for example, but represents the panel skin buckling as if it were on an elastic foundation supplied by the flexible attached flanges, while the web and outstanding flange of the stringer(s) deform but little. During optimization the attached flange will become thicker and/or less wide. Therefore, in the optimum design, the critical local buckling mode will resemble that depicted in Fig. 8 rather than that depicted in Fig. 2.

Figure 3 shows the results from BOSOR4 [50,55] for the same panel. The local buckling load factor from BOSOR4, Lambda(m) = 0.525, with m = 5 representing the critical number of axial halfwaves, is in good agreement with the local buckling load factor predicted from PANDA2 with use of the discretized single module model, Lambda(PANDA2, m=5) = 0.516 (Fig. 2). The small difference is caused by the following differences in the BOSOR4 model [50,55] and the PANDA2 discretized module model:

1. In the PANDA2 model the kinematic relations are for a prismatic structure, whereas in the BOSOR4 model the kinematic relations are for a branched shell of

revolution with a large average radius [55]. (From Fig. 3, the average radius is about 1592 inches).

2. A slightly different discretization is used for each segment in the BOSOR4 model from that used in the PANDA2 model.

OPTIMIZATION WITH STRINGER SPACING "b" HELD CONSTANT AT 10.0 INCHES, THE PANEL IS **PERFECT**, AND LOCAL POSTBUCKLING IS **NOT** PERMITTED

Input data for this case are listed in Tables 2, 7, and 8 of [58]. Figures 4 - 11 pertain to this subsection. Results for the optimized designs are listed in Columns 1 and 2 of Table 3.

Figures 4 - 7, which were generated by the PANDA2 processors called CHOOSEPLOT and DIPLOT (see ITEM 28 of [53]), show results from the first optimization. This optimization was achieved via the part of the runstream listed in Table 2 from "BEGIN" through the four "PANDAOPTs".

Why are four executions of PANDAOPT required in order to obtain an optimum design? The reasons are explained on pp 579 - 582 of [7]. (At the time [7] was written (1987) PANDA2 used the Vanderplaats optimizer called CONMIN whereas now the optimizer is called ADS [56,57], which is the successor to CONMIN. In the example on pp 579 - 582 of [7] IQUICK = 1 (PANDA-type closed form buckling model [59]) whereas here IQUICK = 0 (discretized single module model [7]).) At each successive PANDAOPT the new starting design is the same as the ending design at the previous PANDAOPT. The design point corresponding to the starting design at execution of each of the four PANDAOPTs used for this particular optimization is indicated by an arrow in Fig. 4. Figure 5 displays the evolution of Z-stringer segment widths, b2, h, w (defined in Fig. 1(a) and in Table 1), and Fig. 6 displays the evolution of wall thicknesses, t1, t2, t3, t4, defined in Table 1.

Figure 7 shows all design margins less than unity plotted vs design iteration number. At the optimum design seven margins are critical or almost critical. These are indicated by arrows in the list of margins at the top of Fig. 7.

Margins 1 and 2 are different estimates of the same phenomenon: local buckling as displayed in Fig. 8. A derivation of Margin 2, "Local buckling: Koiter theory", appears in [11]. Margins 5, 20, and 21 represent three different estimates of another phenomenon: overall buckling. Margin 5 is computed with use of a single discretized panel module (Fig. 9) and Margins 20 and 21 are computed for the entire panel width with stringers smeared out in the manner prescribed by Baruch and Singer [49]. (Jaunky, et al [43] apparently have a more accurate method of obtaining "smeared stiffener" stiffness properties for estimating load factors corresponding to general instability. The Jaunky method has not been introduced into PANDA2.) In Margin 20 the string "DONL" means "Donnell theory" and in Margin 21 the string "SAND" means "Sanders theory". For an example in which the Donnell theory and the Sanders theory yield significantly different buckling load factors, see Fig. 1 of [14]. Margin 22 is analogous to Margin 1 except that the critical number of axial halfwaves in this particular case is one rather than five. The m = 1 buckling mode corresponding to Margin 6 is similar to that corresponding to Margin 5 in this case. In principle, Margin 6 is computed with use of membrane stiffness properties corresponding to the locally postbuckled panel. In this particular case, however, there is no post-local buckling because the factor of safety for local buckling is greater than unity. Hence, there is only very, very slight prebuckling deformation in the form of the local buckling mode in this case and hence only a very, very small degree of prebuckling axial "softening" because the amplitude of the local buckling modal initial imperfection [54] is set equal to a very, very small number (Wloc = 0.1E-06).

Figure 8 shows the local buckling mode and load factor and Fig. 9 shows the wide column buckling mode and load factor for the optimized design. As seen from Fig. 8, at the optimum design the local buckling mode from the discretized single-module model closely resembles classical buckling across the width of a flat plate simply supported along the line of intersection of the stringer web to the stringer flange that is attached to the panel skin. Unlike the non-optimized panel, the local buckling mode for which is depicted in Figs. 2 and 3, at the optimum design the attached flange is thick enough not to bend significantly in the widthwise direction in the local buckling mode, as demonstrated in Fig. 8. (Figs. 8 and 9 were obtained from executions of CHOOSEPLOT/DIPLOT following execution MAINSETUP/PANDAOPT for analysis type 3, simulation of a test of a panel of fixed design.) At the optimum design the attached flange is robust enough to

prevent the heel of the stringer from separating from the panel skin.

It often happens that the optimum design determined from a simple sequence of PANDAOPT executions is not a GLOBAL optimum but simply a LOCAL minimum-weight design. Getting trapped at a LOCAL optimum design is probable with gradient-based optimizers such as ADS. The PANDA2 processor called SUPEROPT was introduced to avoid this limitation [14]. During a SUPEROPT run there are many sets of optimizations, each set starting from a different point in design space. Details of the method with examples are given in [14]. While this method does not guarantee the finding of the global optimum design, it makes it unlikely that the value of the objective function corresponding to the final optimum design will be far above the global minimum value. With PANDA2 it is possible to perform several executions of SUPEROPT in sequence, as listed in the bottom part of Table 2. (NOTE: each "SUPEROPT" must be followed by at least one execution of CHOOSEPLOT/DIPLOT).

Results for the final "global" optimum design are listed in Column 2 of Table 3. As seen from comparison of Columns 1 and 2 in Table 3, the panel weight, 51.23 lbs, corresponding to the "local" optimum design (PART 2, Col. 1) is somewhat higher than that corresponding to the "global" optimum design, 49.33 lbs (PART 2, Col. 2). Figures 10 and 11 show the local and wide column buckling modes and load factors for the new optimum design determined via SUPEROPT. Figures 10 and 11 are analogous to Figs. 8 and 9. Note that the new optimum design has a very thick attached flange, t2 = 0.3089 (Column 2 of Table 3). In an actual design process there may exist a manufacturing constraint that does not permit such a thick part. If so, this problem (if it is a problem) can easily be avoided by the user's setting smaller upper bounds on t1, t2, t3, t4 in DECIDE (Table 1).

OPTIMIZATION WITH STRINGER SPACING "b" ALLOWED TO CHANGE, THE PANEL IS **PERFECT**, LOCAL POSTBUCKLING IS **NOT** PERMITTED

Results for this case are listed in Column 3 of Table 3. Note that the optimized panel is considerably lighter (weight = 36.15 lbs, PART 2, Col. 3) than for the two previously obtained optimum designs (weights = 51.23 and 49.33 lbs, PART 2, Cols. 1 and 2).

Note from PARTs 3 - 7, Cols. 1 - 3 in Table 3 that predictions from PANDA2, BOSOR4 and STAGS for local buckling (PARTs 3 - 5) are in good agreement and that predictions from PANDA2 and BOSOR4 for wide column buckling (a good approximation of general instability in this case) are in good agreement (PARTs 6,7). Collapse loads predicted by STAGS significantly exceed the wide column buckling loads predicted by PANDA2 and BOSOR4 because the STAGS model includes the clamping at the two axially loaded edges of the panel whereas both the PANDA2 and BOSOR4 models are based on the assumption of simple support along these two edges in this particular case of a Z-stiffened panel.

Note that for the three cases in which local postbuckling is not permitted the maximum effective stress in each optimized panel is not critical (Table 3, PART 10, Cols. 1 - 3). This is not the case for the remaining seven cases (Cols. 4 - 10) in which local postbuckling is allowed.

OPTIMIZATION WITH STRINGER SPACING "b" ALLOWED TO CHANGE, THE PANEL IS **PERFECT**, LOCAL POSTBUCKLING **IS** PERMITTED, AND LOCAL BUCKLING MODE "JUMPING" **IS** PERMITTED (modejump OFF)

Column 4 of Table 3, PART 1 of Table 4, and Figs. 12 - 22 pertain to this section.

Optimization

Figure 12 shows the evolution of the panel weight during execution of the one SUPEROPT performed in this case. The "modejump" constraint was turned OFF during optimization, that is, incipient mode jumping, a phenomenon modelled in PANDA2 as described in detail in [15], was ignored during optimization. Each "spike" in Fig. 12 represents a new starting design in the SUPEROPT cycle, a starting design generated automatically via the PANDA2 processor called AUTOCHANGE [14]. As explained in [14], the starting designs are generated by random changes in the vector of decision variables consistent with the lower and upper bounds and inequality constraint conditions provided by the PANDA2 user in DECIDE.

Results from PANDA2 for the optimum design

The optimum weight of the panel, 30.07 lbs (Col. 4, PART 2 of Table 3), is about 20 per cent less than that (36.15 lbs) obtained for the optimum design in which local postbuckling is not permitted. The local buckling load factor of the new optimum design, 0.364 (Col. 4, PART 3 of Table 3), indicates that at the design load the optimized panel is loaded well into the local postbuckling regime. The critical number of axial halfwaves in the local buckling mode is 10 [58]. As seen from Col. 4, PART 12 of Table 3 the following design margins are critical or almost so: bending-torsion buckling (-0.001), maximum effective stress (0.016), wide column buckling (0.043), lateral-torsional buckling (-0.030), buckling of stringer segment 4 (outstanding flange, 0.067), buckling of stringer segments 3 and 4 together (web and outstanding flange, -0.002), and general buckling (0.150). (In PANDA2 very small negative margins are permitted for feasible designs).

The margin called "bending-torsion buckling" is computed in exactly the same way as the margin for local buckling, that is, redistribution of stress resultants, Nx, Ny, Nxy, in the panel skin and stringer segments that occurs for loads in excess of the local buckling load is not accounted for in the computation of the "bending-torsion buckling" constraint condition. In contrast, the margin called "lateral-torsional buckling" is computed accounting for this stress redistribution, which is calculated in the "Koiter" (postbuckling) branch of PANDA2 [11]. In this particular case "bending-torsion buckling" is predicted by PANDA2 to occur with two axial halfwaves over the 50-inch length of the panel and "lateral-torsional buckling" is predicted to occur with one axial halfwave. Margins 3 and 10 in PART 16 of Table 16 in [58] appear as follows:

3 -7.31E-04 Bending-torsion buck.(bypassed low-m mode);M=2 ;FS=1.1

10 -2.98E-02 (m=1 lateral-torsional buckling load factor)/(FS)-1;FS=1.1

The margins called "wide column buckling" and "general buckling" are computed with the stress redistribution accounted for. The "wide column buckling" margin is computed from a single discretized module model such as shown in Fig. 11. The "general buckling" margin is computed from a model in which the effect of the stringers is "smeared" (averaged) over the panel width in the manner of Baruch and Singer [49]. The buckling margins called "stringer seg. n" are computed from a PANDA-type (closed form) model [59] in which stringer segment n is assumed to be simply supported along its line of intersection with other segments of the panel module if Segment n represents an "internal" segment (such as the web of the Z) and in which one of the longitudinal edges is considered to be free if Segment n represents an "end" segment (such as the outstanding flange of the Z). The effect of stress redistribution during local postbuckling is accounted for in the computation of these margins.

Values for "local buckling" and "mode jumping" margins are not given in Col. 4, PART 12 of Table 3 because the PANDA2 user has indicated in the PANDA2 input data for MAINSETUP that these phenomena should not constrain the design in this particular case. The "local buckling" margin becomes non-critical because the PANDA2 user has set the factor of safety for local buckling equal to 0.3. (See Margin No. 1 listed in PART 16 of Table 16 in [58]).

Figure 13 shows how the single discretized, optimized panel module deforms, according to PANDA2, as the panel is loaded beyond the local buckling load. Figure 14 shows how the local buckles grow and how the postbuckled panel bows with increasing axial compression, Nx. Since there is essentially zero initial local buckling modal initial imperfection (Wloc = 0.1E-06 in Table 17 of [58]), there is an abrupt change in behavior at the local buckling load factor, Nx(cr) = -2000 x 0.364 = -728 lb/in. The "corner" becomes rounded off when there exists a local buckling modal initial imperfection with a significant amplitude (See Fig. 126 of [58], for example). These figures were generated with ITYPE = 3 (test simulation mode of analysis) in MAINSETUP and with use of the PANDA2 processors, CHOOSEPLOT and DIPLOT, for generation of the graphics.

Comparison of predictions from PANDA2 and STAGS for the optimum design

The PANDA2 processor called STAGSMODEL [12] makes it relatively easy to generate input data for STAGS [52] corresponding to a panel previously optimized by PANDA2. In this way, the quality of the optimum design obtained by PANDA2 can be evaluated by comparison with predictions from a

general-purpose finite element computer program that does not use the many "tricks" and approximations employed in PANDA2 in order to save computer time.

At present, STAGSMODEL works only for panels that are clamped along the two axially loaded edges and only for panels that do not contain any transverse stiffeners (rings). STAGSMODEL produces the two STAGS input files, *.bin and *.inp, for what in STAGS jargon is called an "element unit" (no "shell units"). Therefore, the *.inp file is often very large (more than a megabyte). Typical input data for STAGSMODEL are listed in Table 12 of [58]. In this particular case the STAGS finite element model consists of only a single module. Therefore, the STAGS model is analogous to the PANDA2 model shown in Fig. 13. A one-module model is acceptable in this case because the panel is not subjected to in-plane shear loading and the walls of the panel skin and Z-stiffener are not anisotropic.

In the STAGS models generated during this study the two longitudinal edges are free to approach eachother and to undergo in-plane warping. This freedom of displacement along these edges generally leads to conservative results because the local buckles can become deeper in the postbuckling regime than would be the case if in-plane warping of the two longitudinal edges were prevented.

From linear analysis STAGS predicts a critical bifurcation buckling eigenvalue, pcr = 0.37208 (Fig. 15), which is in very good agreement with PANDA2's prediction of 0.364 (Col. 4, PART 3 of Table 3). As seen in Fig. 15(b) the local buckling mode from STAGS has 9 axial halfwaves, whereas PANDA2 predicts 10 axial halfwaves. The difference arises from the different boundary conditions used in the STAGS (clamped) and PANDA2 (simple support) at the two axially loaded ends of the panel module for the analysis of local buckling. In the central region of the panel the axial wavelengths of the local buckles as predicted by STAGS and PANDA2 are in very good agreement.

Next, it is necessary to find at what load STAGS predicts the optimized panel to collapse under uniform axial end shortening. The method of doing this is described in some detail in [12]. A nonlinear collapse analysis is performed with STAGS with use of the one-module model shown in Fig. 15. The STAGS model includes an initial imperfection in the form of the local buckling mode depicted in Fig. 15. This initial imperfection is required to avoid almost singular behavior in the neighborhood of the local buckling load at a load factor of about 0.372. With a small imperfection in the form of the local buckling mode there will be a smooth transition from prebuckling state to locally postbuckled state as the panel is loaded into its post-local-buckling regime. (See Fig. 6 of [11] for an example).

NOTE: In this paper for all the STAGS results a load factor, PA = 1.0, corresponds to the design load, Nx = -2000 lb/in.

Figure 16 shows the load-end-shortening curve obtained via STAGS. As demonstrated in Fig. 17 there are several groups of load steps for which unloading occurs. Often in a case such as this the unloading represents "Riks reversal" (see Fig. 17 of [15]), in which the Riks path [60] doubles back on itself, converging to the same states determined in previous load steps. Superficially that appears to be the case here, since all the points in Fig. 16 appear to lie on the same fundamental curve. However the points do NOT all lie on the same fundamental curve. As will be shown next, the equilibrium state at Point 23 is not the same as that at Point 76, for example. (Compare Figs. 18(d) and 18(e)).

Figures 18(a) and 18(d) show the deformed state of the panel module at a load factor very near unity (PA = 1.00832), that is, very near the design load at Load Step 23. While the skin is deformed in a pattern similar to that shown in Fig. 15(b) (local buckling mode shape), the stringer undergoes a long-axial-wave sidesway similar to the deformation patterns corresponding to Margin Numbers 3 and 10 in PART 16 of Table 16 of [58]:

3 -7.31E-04 Bending-torsion buck.(bypassed low-m mode);M=2 ;FS=1.1

10 -2.98E-02 (m=1 lateral-torsional buckling load factor)/(FS)-1;FS=1.1

Figures 18(b-e) display edge-on views of the locally postbuckled panel module at four load steps, Steps 10, 15, 23, and 76. Note that the deformations shown in Figs. 18(a-d) (Load Steps 10, 15, 23) represent essentially growth of the local buckling lobes as the loading is increased. However, the equilibrium state of the panel at Load Step 76 is quite different from that at Load Step 23, even though the load factor PA is, for all practical purposes, the same at these two load steps. At Load Step 76 the local buckling lobes along the far edge of the panel module have shifted relative to those

along the near edge.

Figures 19(a,b), which are "fringe" plots of the normal displacement w in the panel skin as viewed from the surface of the panel skin opposite to the surface to which the stringer is attached, show more clearly the relative positions of the local buckling lobes on either side of the stringer at Load Steps 23 and 76. Note that at Load Step 76 (Fig. 19(b)) an additional buckle has appeared along the bottom half of the single panel module relative to the number of buckles apparent there at Load Step 23 (Fig. 19(a)). This change in equilibrium state represents a mode "jump". Often a mode "jump" can be captured only by means of a nonlinear transient STAGS run "sandwiched" between nonlinear static STAGS runs [15]. In this case it turns out that the static Riks procedure [60] is capable of capturing the change in state of the panel between Load Step 23 and Load Step 76 (Fig. 17). As will be seen later, this mode "jump" has a significant influence on the maximum effective stress generated in the panel skin.

Figure 20 demonstrates the local buckling and postbuckling phenomenon at a location along the axis of the panel, x = 30 inches from one end. The depth of the buckles is equal to the difference between the normal displacement w at either of the two longitudinal edges (curves with triangles and squares) and w in the panel skin under the stringer web (curve with circles). Up to Load Step 23 the buckle depth as a function of load obtained by STAGS agrees reasonably well with the prediction by PANDA2 shown in Fig. 14 as the curve with squares. After Load Step 23 it is clear that the buckle represented by the curves with triangles in Fig. 20 shifts along the panel axis, so that what was a maximum w(x) at Load Step 23 becomes a node (w(x)=0) for Load Step 58 in Fig. 20. The different axial positions of the local buckles along the longitudinal edge of the panel module represented by the curves with triangles in Fig. 20 are displayed for Load Steps 23 and 76 in the fringe plots of Figs. 19(a,b) corresponding to the bottommost of the two longitudinal edges.

Figure 21 shows sidesway of the stringer at the panel end (curve with squares) and at the panel midlength (curve with circles). Sidesway at the panel ends begins immediately after local buckling, a phenomenon that cannot be predicted by the PANDA2 analysis. Sidesway at the panel midlength begins at a somewhat higher load. This also cannot be predicted by the PANDA2 analysis, which is based on the assumption that in the post-local buckling regime the panel module cross section deforms as shown in Fig. 13. According to PANDA2, sidesway of the stringer will exist in this case of a perfect panel only at loads in excess of the design load because the following margins listed in Part 16 of Table 16,

3 -7.31E-04 Bending-torsion buck.(bypassed low-m mode);M=2 ;FS=1.1

10 -2.98E-02 (m=1 lateral-torsional buckling load factor)/(FS)-1;FS=1.1

become significantly negative only for loads in excess of 1.1 times the design load, Nx = -2000 lb/in.

Figures 90 - 95 of [58] show extreme fiber effective (von Mises) stress vs load factor PA where fringe plots (not included because they are inadequate in black-and-white) indicate that these stresses are the highest of any in the single panel module and at which PANDA2 predicts that maxima occur in the single discretized module model. The values of these stresses at the design load, PA = 1.0, before the mode "jump" (at Load Step 23) can be compared with the values predicted by PANDA2. This comparison appears in PART 1 of Table 4.

PANDA2 rather grossly underestimates the maximum effective stress midway between stringers (discussed later in connection with Fig. 27) but the effective stress at this location is not critical. PANDA2 overestimates the critical effective stress anywhere in the panel by about 10 per cent.

The effective stresses from the STAGS model listed in PART 1 of Table 4 correspond to Load Step 23, that is, at the design load, PA = 1.0 but before mode jumping occurs. Figure 22 demonstrates the extremely harmful effect of mode jumping. The maximum effective stress in the panel skin at the rivet line becomes unacceptably high at loads below the design load as the postbuckling pattern changes between Load Step 23 and Load Step 76. Whereas PANDA2 predicts "stress failure" (defined here as the maximum effective stress reaching the value 45 ksi) at a load factor of 1.016 (Col. 4, PART 10 of Table 3), the STAGS model predicts "stress failure" at a load factor of approximately 0.91 (Col. 4, PART 11 of Table 3). PANDA2 yields unconservative stress constraints if optimization is performed with the "modejump prevention switch" turned OFF.

Therefore, the optimum design should be obtained with the "modejump prevention switch" turned ON. The

results for this next optimization and subsequent analysis of the optimized panel are given in the next section.

OPTIMIZATION WITH STRINGER SPACING "b" ALLOWED TO CHANGE, THE PANEL IS **PERFECT**, LOCAL POSTBUCKLING **IS** PERMITTED, AND LOCAL BUCKLING MODE "JUMPING" IS **NOT** PERMITTED (modejump ON)

Column 5 in Table 3, PART 2 of Table 4, and Figs. 23 - 27 pertain to this section. From Col. 5, PART 2 of Table 3 we see that optimization with the "modejump prevention switch" turned ON causes the optimum weight to increase from 30.07 to 32.21 lbs. At the new optimum design the local buckling load factor is now 0.639 (compare with 0.364 for the optimum design with the "modejump prevention switch" turned OFF). The new design has stringers closer together (b = 5.00 in. vs b = 5.94 in. for the optimum design with the "modejump prevention switch" turned OFF) and with thicker panel skin (t1 = 0.0831 in. vs t1 = 0.0680 in.) and narrower outstanding flange (w = 0.539 in. vs w = 0.907 in.).

Figure 23, the load-end-shortening curve corresponding to the new optimum design, is analogous to Fig. 16; Fig. 24 is analogous to Fig. 21; and Fig. 25 is analogous to Fig. 22. Figure 26 shows the collapse mode of the panel according to STAGS. Figure 26(d) is analogous to Fig. 18(a). In this case the lateral-torsional collapse mode has three axial halfwaves (Fig. 26(e)), whereas the lateral-torsional collapse mode for the optimum design obtained with the "modejump prevention switch" turned OFF has only one axial halfwave (Fig. 18(a)). These STAGS predictions are in agreement with those for the lateral-torsional buckling mode from PANDA2.

In the new design there is no dramatic shift of the local buckles on one side of the stringer with respect to those on the other side of the stringer for load factors below 1.11 (Fig. 26(b)). Hence, there is no "mode jumping" below or near the design load factor (PA = 1.0), according to both PANDA2 and STAGS for the new design.

The maximum effective stresses in the panel at the design load, Nx = -2000 lb/in, are listed in PART 2 of Table 4. As before (PART 1 of Table 4), PANDA2 rather severely underestimates the maximum effective stress midway between stringers. In this case the maximum effective stress predicted by PANDA2 occurs in the web at the web root and overestimates that predicted by STAGS at the same location by about 20 per cent.

While the maximum effective stress in the optimized panel is not critical at the design load, according to STAGS it increases steeply for load factor PA in excess of 1.0, as seen from Fig. 25, from which it is clear that the maximum effective stress becomes critical (45 ksi) at a load factor of about 1.1. The rather abrupt change in slope of the plots of effective stress near the design load PA = 1.0 is caused by the abrupt change in rate of stringer sidesway evident in Fig. 24.

Note, from Cols. 4 and 5, PART 9 of Table 3, that for the initially perfect optimized panels in which local postbuckling is permitted, the collapse load factors according to STAGS (1.25 and 1.35) are much closer to the design load factor, PA = 1.0, than is the case for the optimized panels in which local postbuckling is not permitted (Cols. 1-3: 2.3, 1.72, 1.62). It is this closeness that justifies the replacement of clamping at the two axially loaded edges with classical simple support in the PANDA2 models in the case of Z-stiffened panels.

RESULTS FOR PANELS WITH INITIAL GENERAL BUCKLING MODAL IMPERFECTION

Columns 6 - 10 in Table 3 and PARTs 3 - 6 in Table 4 pertain to this section. More details about these cases appear in [58]. Some comments about these results are:

1. The presence of the global initial imperfection of amplitude plus or minus 0.1 in. causes the weight of the optimized Z-stiffened panel to increase from 32.21 lbs (Col. 5) to 35.22 lbs (Col. 7).

2. The predictions of maximum effective stress from PANDA2 are conservative relative to those from STAGS (Cols. 6-10, PARTs 10,11) but not too conservative.

3. Lateral-torsional buckling is critical for all optimum designs.

4. The load factors from STAGS for local buckling of the imperfect panels are not as close to those from PANDA2 (Cols. 6 - 10, PARTs 5 and 3) as is the case

for the perfect (unbowed) panels (Cols. 1 - 5). This discrepancy is caused by the fact that prebuckling growth of the initial imperfection is accounted for in the PANDA2 model but not in the STAGS model for linear bifurcation buckling, from which the values in PART 5 of Table 3 were generated. The purpose of the STAGS linear bifurcation runs is only to obtain initial local buckling imperfection shapes in order to avoid numerical difficulties in the subsequent collapse analyses with STAGS.

5. The optimized J-stiffened and T-stiffened panels, which are assumed to have attached flanges that are bonded rather than riveted to the panel skin , weigh significantly less than the optimized Z-stiffened panels. (See Cols. 9 and 10, PART 2). As might be expected from the bilateral symmetry of the T-stiffener, the optimized weight of the T-stiffened panel is less than that for the J-stiffened panel.

6. The widths of the outstanding flanges of the imperfect Z-stiffened panels are greater than those for the perfect Z-stiffened panels.

7. If a **clamped** panel is optimized with a negative bowing imperfection (Col. 7) the same panel will survive a positive bowing imperfection of the same amplitude (Col. 8). This is because, in the case of a clamped globally imperfect panel, PANDA2 checks for conditions both at the panel midlength and at the panel ends. Negative bowing of an axially compressed panel creates at the midlength more axial compression in the panel skin than at the stringer tips. At the panel ends the reverse holds. Reversal of sign of the bowing imperfection simply changes the order in which the various buckling and stress constraints are processed by PANDA2.

WHAT ABOUT PANDA2's UNCONSERVATIVE STRESS PREDICTIONS FOR POINTS MIDWAY BETWEEN STRINGERS?

PARTS 1 - 4 and 6 of Table 4 demonstrate that, for points in the panel skin midway between stringers, PANDA2 significantly underestimates the maximum effective stress compared with predictions from STAGS for the one-module STAGS model in which the two longitudinal edges do not have to remain straight and are free to approach eachother. However, in all of these cases the maximum effective stress at these points is always less than the critical effective stress (45 ksi) and usually less than the maximum effective stress at other locations in the panel module at the design load, Nx = -2000 lb/in (STAGS load factor PA = 1.0).

Figure 27 shows the behavior of the maximum effective stress midway between stringers according to STAGS for the perfect Z-stiffened panel optimized with the "modejump prevention switch" turned ON (Col. 5 of Table 3, PART 2 of Table 4). Local buckling occurs at a load factor of 0.639. Note that for load factors PA between 1.0 and 1.2 the effective stress stops increasing and starts to decrease dramatically as the panel buckles locally and load is shed from the panel skin in the region midway between stringers to the stringers and to the panel skin in the neighborhoods of the stringers. In contrast, the maximum stress at points in and near the stringers increases monotonically, as shown in Fig. 25, for example. It is felt that for most practical optimized designs in which local postbuckling of the panel skin is permitted, the "worst" stresses will occur near and in the stringer segments rather than near the midwidth of the bays between stringers.

CONCLUSIONS

The agreement between PANDA2 and STAGS appears to be sufficient to qualify PANDA2 as a preliminary design tool for panels with riveted Z-shaped stringers for service in the locally postbuckled regime. With proper (conservative) user input, such as specification that the mode jump constraint be turned ON during optimization cycles, PANDA2 errs on the conservative side, but does not appear to be overly conservative. Further work should include a similar study performed for laminated composite panels, for cylindrical panels, and for panels with both strigners and rings.

ACKNOWLEDGMENTS

The author wishes to express his appreciation for the continuing support of Dr. T. J. Kertesz, Director, Satellite Integration (Department E9-01) in Lockheed Martin Missiles and Space Satellite Systems Division. Mr. Bill Bushnell helped the author provide the proper format of the paper for the AIAA and continues to support the author in the maintenance of the PANDA2 program on several UNIX-based workstations. Bill Bushnell wrote the software PLOTPS by means of which all of the "x,y" types of plots in this paper were

generated. The author is grateful to Dr. Charles Rankin and Mr. Frank Brogan, developers of the STAGS program, for their helpful suggestions on the use of STAGS.

REFERENCES

[1] van der Neut, A, "Overall buckling of Z-stiffened panels in compression", Delft University of Technology, Dept. of Aerospace Engineering, Report LR303, August 1980

[2] Wittrick, W. H., "A unified approach to the initial buckling of stiffened panels in compression", Aeronautical Quarterly, Vol. 19, pp 265-283 (1968)

[3] Williams, F. W. and Wittrick, W. H., "Computational procedures for a matrix analysis of the stability and vibration of thin flat-walled structures in compression", International Journal of Mechanical Sciences, Vol. 11, pp. 979-998 (1969)

[4] Riks, E., "A buckling analysis of a Z-stiffened compression panel simply supported on equidistant ribs", National Aerospace Laboratory NLR, The Netherlands, Report NLR TR 78145 L, December, 1978

[5] B. O. Almroth and F. A. Brogan, The STAGS Computer Code, NASA CR-2950, NASA Langley Research Center, Hampton, VA (1978).

[6] Viswanathan, A. V. and Tamekuni, M., "Elastic buckling analysis for composite stiffened panels and other structures subjected to biaxial inplane loads", NASA CR-2216, September 1973

[7] D. Bushnell, "PANDA2-Program for minimum weight design of stiffened, composite, locally buckled panels", Computers and Structures, Vol. 25 (1987) pp. 469-605.

[8] J. N. Dickson, S. B. Biggers, and J. T. S. Wang, "Preliminary design procedure for composite panels with open-section stiffeners loaded in the post-buckling range," in: Advances in Composite Materials, A. R. Bunsell, et al,editors, Pergamon Press Ltd., Oxford, England, 1980, pp 812-825. Also see, J. N. Dickson and S. B. Biggers, "POSTOP: Postbuckled open- stiffened optimum panels, theory and capability", NASA Langley Research Center, Hampton, Va., NASA Contractor Report from NASA Contract NAS1 - 15949, May 1982.

[9] Butler, R. and Williams, F. W., "Optimum design features of VICONOPT, an exact buckling program for prismatic assemblies of anisotropic plates," AIAA Paper 90-1068-CP, Proceedings 31st AIAA/ASME Structures, Structural Dynamics, and Materials Meeting, pp 1289-1299. Also see Williams, F. W., Kennedy, D., Anderson, M.S., "Analysis features of VICONOPT, an exact buckling and vibration program for prismatic assemblies of anisotropic plates,", AIAA Paper 90-0970-CP, Proceedings 31st AIAA/ASME Structures, Structural Dynamics, and Materials Meeting, pp 920-929. Also see Kennedy, D., Powell, S. and Williams, F., "Local postbuckling analysis for perfect and imperfect longitudinally compressed plates and panels", AIAA-98-1770, 39th AIAA/ASME Structures, Structural Dynamics, and Materials Meeting, 1998.

[10] M. S. Anderson and W. J. Stroud, "General panel sizing computer code and its application to composite structural panels," AIAA Journal, 17, (1979) pp. 892-897. Also see W. J. Stroud and M. S. Anderson, "PASCO: Structural panel analysis and sizing code, capability and analytical foundations," NASA TM-80181, NASA Langley Research Center, Hampton, Va., 1981. Also see W. J. Stroud, W. H. Greene and M. S. Anderson, "Buckling loads of stiffened panels subjected to combined longitudinal compression and shear: Results obtained with PASCO, EAL, and STAGS computer programs," NASA TP 2215, Nasa Langley Research Center, Hampton, Va., January 1984.

[11] Bushnell, D., "Optimization of composite, stiffened, imperfect panels under combined loads for service in the postbuckling regime", Computer Methods in Applied Mechanics and Engineering, Vol. 103, pp 43-114 (1993)

[12] Bushnell, D. and Bushnell, W. D., "Minimum-weight design of a stiffened panel via PANDA2 and evaluation of the optimized panel via STAGS", Computers and Structures, Vol. 50, no. 4, p569-602 (1994)

[13] Bushnell, D. and Bushnell, W. D., "Optimum design of composite stiffened panels under combined loading", Computers and Structures, Vol. 55, No. 5, pp 819-856 (1995)

[14] Bushnell, D., "Recent enhancements to PANDA2"

37th AIAA Structures, Structural Dynamics and Materials Conference, April, 1996.

[15] Bushnell, D., Rankin, C. C., and Riks, E., "Optimization of stiffened panels in which mode jumping is accounted for", AIAA Paper 97-1141, Proceedings 38th Structures, Structural Dynamics and Materials Conference, pp 2133-2162, 1997

[16] Stein, M, "The phenomenon of change of buckling patterns in elastic structures,", NASA Technical report R-39, NASA (1959)

[17] A. W. Leissa, "Buckling of laminated composite plates and shell panels," AFWAL-TR-85-3069, Air Force Wright Aeronautical Laboratories, Wright-Patterson AFB, Ohio 45433, June, 1985.

[18] R. R. Arnold and J. C. Parekh, "Buckling, postbuckling, and failure of flat and shallow-curved, edge-stiffened composite plates subject to combined axial compression and shear loads", Presented at 27th SDM Meeting, San Antonio, Tx., April 1986, AIAA Paper No. 86-1027-CP, 1986, Proceedings pp. 769-782.

[19] J. H. Starnes,Jr., N. F. Knight,Jr. and M. Rouse, "Postbuckling behavior of selected flat stiffened graphite- epoxy panels loaded in compression," AIAA Paper 82-0777, presented at AIAA 23rd Structures, Structural Dynamics, and Materials Conference, New Orleans, May, 1982. See also, AIAA J., 23, (8) (1985) pp.1236-1246.

[20] E. E. Spier, "On experimental versus theoretical incipient buckling of narrow graphite/epoxy plates in compression," Proc. AIAA 21st SDM Conference, AIAA Paper 80-0686-CP, May, 1980.

[21] E. E. Spier, "Local buckling, postbuckling, and crippling behavior of graphite-epoxy short thin-walled compression members," Naval Air Systems Command, Washington, D. C., NASC-N00019-80-C-0174, July 1981.

[22] N. R. Bauld, Jr. and N. S. Khot, "A numerical and experimental investigation of the buckling behavior of composite panels", Computers and Structures, 15 (1982) pp. 393-403.

[23] N. S. Khot and N. R. Bauld, Jr., "Further comparison of the numerical and experimental buckling behaviors of composite panels," Computers and Structures, 17, (1983) pp. 61-68.

[24] Y. Zhang and F. L. Matthews, "Postbuckling behavior of anisotropic laminated plates under pure shear and shear combined with compressive loading", AIAA Journal, 22, (2), (1984) pp 281-286.

[25] Stoll, F. and Gürdal, Z., "Nonlinear analysis of compressively loaded linked-plate structures," AIAA Paper 90-0968-CP, Proceedings 31st AIAA/ASME Structures, Structural Dynamics, and Materials Meeting, pp 903-913 (1990).

[26] Stoll, F. and Gürdal, Z., and Starnes, J. H., Jr., "A method for the geometrically nonlinear analysis of compressively loaded prismatic composite structures," VIPSU Center for Composite Materials and Structures Report CCMS-91-03 (VPI-E-91-01), February, 1991

[27] Shin, D. K., Gürdal, Z., and Griffin, O. H., Jr., "Minimum weight design of laminated composite plates for postbuckling performance," AIAA Paper 91-0969-CP, Proceedings 32nd AIAA/ASME Structures, Structural Dynamics, and Materials Meeting, pp 257-266 (1991)

[28] Ley, R.P., Gürdal, Z., and Johnson, E.R. (1993). Optimal design of imperfect, anisotropic, ring-stiffened cylinders under combined loads. AIAA Paper 93-1526-CP, Proceedings of 34th AIAA Structures, Structural Dynamics, and Materials Conference, Part 4, pp 1881-1889.

[29] Ley, R.P., Johnson, E.R., and Gürdal, Z. (1992). Buckling of imperfect, anisotropic, ring-stiffened cylinders under combined loads. AIAA Paper 92-2232-CP, Proceedings of 33rd AIAA Structures, Structural Dynamics, and Materials Conference, Part 1, pp 86-94.

[30] Nagendra, S., Haftka, R. T., and Gürdal, Z. (1992). Stacking sequence optimization of simply supported laminates with stability and strain constraints. AIAA Paper 92-2310-CP, Proceedings of 33rd AIAA Structures, Structural Dynamics, and Materials Conference, Part 5, pp. 2526-2535.

[31] Ragon, S. A., Gürdal, Z, Haftka, R.T., and Tzong, T. J., "Global/local structural wing design using response surface techniques", AIAA Paper 97-1051, Proceedings of 38rd AIAA Structures, Structural Dynamics, and Materials Conference, Part 2, pp 1204-1214.

[32] Venkataraman, S. and Haftka, R. T., "Integration of finite element analysis program and panel design

program", AIAA Paper 97-1052, Proceedings of 38rd AIAA Structures, Structural Dynamics, and Materials Conference, Part 2, pp 1215-1224.

[33] Le Riche, R. and Haftka, R. T. (1992). Optimization of laminate stacking sequence for buckling load maximization by genetic algorithm. AIAA Paper 92-2314-CP, Proceedings of 33rd AIAA Structures, Structural Dynamics, and Materials Conference, Part 5, pp. 2564-2575.

[34] Lombardi, M., Haftka, R. T., and Cinquini, C. (1992). Optimization of composite plates for buckling by simulated annealing. AIAA Paper 92-2313-CP, Proceedings of 33rd AIAA Structures, Structural Dynamics, and Materials Conference, Part 5, pp. 2552-2563.

[35] Vitali, R., Park, O, Haftka, R. T., and Sankar, B. V., "Structural optimization of a hat stiffened panel by response surface techniques", AIAA Paper 97-1151, Proceedings of 38th AIAA Structures, Structural Dynamics, and Materials Conference (1997)

[36] Park, O, Haftka, R. T., Sankar, B. V., and Nagendra, S., "Analytical and experimental study of a blade-stiffened panel in axial compression", AIAA Paper 98-1993, Proceedings of 39th AIAA Structures, Structural Dynamics, and Materials Conference (1998)

[37] Librescu, L. and Chang, M.-Y. (1993). Effects of geometric imperfections on vibration of compressed shear deformable laminated composite curved panels. Acta Mechanica, 96, 203-224.

[38] Librescu, L. and Souza, M. A. (1991). Postbuckling behavior of shear deformable flat panels under the complex action of thermal and in-plane mechanical loadings. AIAA Paper 91-0913-CP, Proceedings of 32rd AIAA Structures, Structural Dynamics, and Materials Conference, Part 2, pp. 917-925.

[39] Librescu, L. and Stein, M. (1991). A geometrically nonlinear theory of transversely isotropic laminated composite plates and its use in the post-buckling analysis. Thin-Walled Structdures, 11, 177-201.

[40] Graves-Smith, T.R. and Sridharan, S., "A finite strip method for the post-locally-buckled analysis of plate structures," Int. J. Mech. Sci., Vol. 20, pp 833-843 (1978)

[41] Peng, M-H and Sridharan, S., "Optimized design of stiffened panels subject to interactive buckling," AIAA Paper 90-1067-CP, Proceedings 31st AIAA/ASME Structures, Structural Dynamics, and Materials Meeting, pp 1279-1288 (1990).

[42] Jaunky, N, Knight, N. F., and Ambur, D. R., "Buckling of arbitrary quadrilateral anisotropic plates", AIAA Journal, Vol. 33, pp 938-944 (1995)

[43] Jaunky, N., Knight, N. F. and Ambur, D., "Formulation of an improved smeared stiffener theory for buckling analysis of grid-stiffened composite panels", Composite: Part B (formerly International J. for Composite Engineering), Vol. 27B, No. 5, pp 519-526 (1996)

[44] Jaunky, N., Knight, N. F., and Ambur, D. R., "Optimal design of general stiffened composite circular cylinders for global buckling with strength constraints", AIAA Paper 97-1402, Proceedings 38th AIAA/ASME Structures, Structural Dynamics, and Materials Meeting, pp 2521-2531 (1997).

[45] Meyers, C. A. and Hyer, M. W. (1992). Thermally-induced, geometrically nonlinear response of symmetrically laminated composite plates. AIAA Paper 92-2539-CP, Proceedings of 33rd AIAA Structures, Structural Dynamics, and Materials Conference, Part 2, pp. 1027-1037.

[46] Nemeth, M. P. (1992). Buckling behavior of long symmetrically laminated plates subjected to compresion, shear, and inplane bending loads. AIAA Paper 92-2286-CP, Proceedings of 33rd AIAA Structures, Structural Dynamics, and Materials Conference, Part 2, pp. 274-282.

[47] Noor, A. K., Starnes, J. H., Jr., and Peters, J. M. (1992). Thermomechanical buckling and postbuckling of multilayered composite panels. AIAA Paper 92-2541-CP, Proceedings of 33rd AIAA Structures, Structural Dynamics, and Materials Conference, Part 2, pp. 1052-1068.

[48] McGowan, D. M. and Anderson, M. S., "Development of curved-plate elements for the exact buckling analysis of composite plate assemblies including transverse shear effects", AIAA Paper 97-1305, Proceedings 38th AIAA/ASME Structures, Structural Dynamics, and Materials Meeting, pp 2678-2692 (1997).

[49] Baruch, M. and Singer, J., "Effect of eccentricity of stiffeners on the general instability of stiffened cylindrical shells under hydrostatic pressure," Journal of Mechanical Engineering Science, 5, (1) (1963) pp.23-27.

[50] D. Bushnell, "BOSOR4: Program for stress, buckling, and vibration of complex shells of revolution," Structural Mechanics Software Series - Vol. 1, (N. Perrone and W. Pilkey, editors), University Press of Virginia, Charlottesville, 1977, pp. 11-131. See also Computers and Structures, Vol. 4, (1974) pp. 399-435; AIAA J, Vol. 9, No. 10, (1971) pp. 2004-2013; Structural Analysis Systems, Vol. 2, A. Niku-Lari, editor, Pergamon Press, Oxford, 1986, pp. 25-54, and Computers and Structures, 18, (3), (1984) pp. 471-536.

[51] W. T. Koiter, "Het Schuifplooiveld by Grote Overshrijdingen van de Knikspanning," Nationaal Luchtvaart Laboratorium, The Netherlands, Report X295, November 1946 (in Dutch).

[52] C. C. Rankin, P. Stehlin, and F. A. Brogan, "Enhancements to the STAGS computer code", NASA CR 4000, NASA Langley Research Center, Hampton, VA (1986).

[53] D. Bushnell, .../panda2/doc/panda2.news, a continually updated file distributed with PANDA2 that contains a log of all significant modifications to PANDA2 from 1987 through the present.

[54] Bushnell, D., "Approximate method for the optimum design of ring and stringer stiffened cylindrical panels and shels with local, inter-ring and general buckling modal imperfections", Computers and Structures, Vol. 59, pp. 489-527 (1996)

[55] Bushnell, D., "Stress, buckling and vibration of prismatic shells", AIAA Journal, Vol. 9, No. 10, (1971) pp 2004-2013

[56] Vanderplaats, G. N., "ADS--a FORTRAN program for automated design synthesis, Version 2.01", Engineering Design Optimization, Inc, Santa Barbara, CA, January, 1987

[57] Vanderplaats, G. N. and Sugimoto, H., "A general-purpose optimization program for engineering design", Computers and Structures, Vol. 24, pp 13-21, 1986

[58] Bushnell, D., "Optimization of panels with riveted Z-shaped stiffeners via PANDA2", LMCO-P489100, Lockheed-Martin Missiles and Space Co., Palo Alto, CA (October 1997)

[59] D. Bushnell, "Theoretical basis of the PANDA computer program for preliminary design of stiffened panels under combined in-plane loads," Computers and Structures, Vol. 27, No. 4, pp 541-563 (1987)

[60] Riks, E., Brogan, F. A., and Rankin, C. C., "Aspects of the stability analysis of shells" in STATIC and DYNAMIC STABILITY OF SHELLS (W. B. Kratzig and E. Onate, editors), Springer Series in Computational Mechanics, Springer-Verlag, Heidelberg (1990)

[61] Park, O., Haftka, R., Sankar, B., and Nagendra, S., "Analytical and experimental study of a blade stiffened panel in axial compression", 39th AIAA/ASME Structures, Structural Dyamics, and Materials Meeting, AIAA 98-1993, 1998

[62] Wiggenraad, J., Arendsen, P., and da Silva Pereira, J. M., "Design Optimization of stiffened composite panels with buckling and damage tolerance constraints", 39th AIAA/ASME Structures, Structural Dynamics, and Materials Meeting, AIAA 98-1750, 1998.

Table 1 Panel to be optimized by PANDA2 (blade stiffened, aluminum)

Overall length of the panel	L1 = 50 in.	
Overall width of the panel	L2 = 50 in.	
Young's modulus,	E = 10 msi	
Poisson ratio	nu = 0.3	
Weight density	rho = 0.1 lb/in**3	
Maximum allowable effective stress	SIGBAR = 45 ksi	
Boundary conditions:	clamped along two axially loaded edges simple support along two unloaded edges	
Applied load	Nx = -2000 lb/in	

DECISION VARIABLES (inches)	LOWER BOUND	INITIAL VALUE	UPPER BOUND
b = stringer spacing	5.0	10.0	10.0
b2 = width of attached flange	1.0	3.0	5.0
h = height of web	0.5	3.0	5.0
w = width of outstanding flange	0.5	3.0	5.0
t1 = thickness of panel skin	0.01	0.15	0.5
t2 = thickness of attached flange	0.01	0.05	0.5
t3 = thickness of web	0.01	0.10	0.5
t4 = thickness of outstanding flange	0.01	0.10	0.5

Table 2 Sequence of PANDA2 commands used to obtain an optimum design

Command	function performed by command
BEGIN	(Provide starting design; input data listed in Table 2 in [58])
SETUP	(Set up matrix templates. no input data required. See Ref. [7])
DECIDE	(Choose decision variables and bounds. Table 7 in [58])
MAINSETUP	(Choose loading, analysis type, model type... Table 8 in [58])
PANDAOPT	("batch" execution of PANDA2 mainprocessor. See Ref. [7])
PANDAOPT	"
PANDAOPT	"
PANDAOPT	"
CHOOSEPLOT	(Choose which decision variables, margins to plot. See [53])
DIPLOT	(Obtain plots. See Refs. [12,13])
SUPEROPT	(Attempt to find global optimum design. See Ref. [14])
CHOOSEPLOT	
DIPLOT	
SUPEROPT	
CHOOSEPLOT	
DIPLOT	
SUPEROPT	
.	
.	
.	

Table 3 Summary of results for various optimum designs from PANDA2, BOSOR4, and STAGS (Dimensions in inches)

PART 1: CHARACTERISTICS OF CASE										
Was SUPEROPT used?-->	no	yes	yes	yes	yes	yes	no	yes	yes	
Local postbuckling?->	no	no	no	yes	yes	yes	yes	yes	yes	yes
Stringer spacing---->	10in.	10in.	var.	var.	var.	var.	var.	var.	var.	var.
Bowing Imperfection->	0	0	0	0	0	-0.1	-0.1	+0.1	-0.1	-0.1
Stringer type------->	Z	Z	Z	Z	Z	Z	Z	Z	J	T
Modejump constraint->	-	-	-	OFF	ON	OFF	ON	ON	ON	ON
Table number [58]--->	9	14	15	16	18	19	20	21	22	23
Column number------->	1	2	3	4	5	6	7	8	9	10
PART 2: OPTIMUM DESIGN OF 50 in. x 50 in. PANEL										
panel weight (lbs)	51.23	49.33	36.15	30.07	32.21	33.49	35.22	35.22	31.08	29.58
WIDTHS (in.):										
stringer spacing,b	10.00	10.00	5.00	5.94	5.00	6.25	5.19	5.19	7.31	6.06
attached flange, b2	1.00	1.00	1.00	1.14	1.00	1.06	1.00	1.00	2.06	2.02
stringer height, h	2.00	2.62	2.17	2.35	2.29	2.30	2.19	2.19	2.22	1.69
outstandng flnge,w	1.42	0.723	0.500	0.907	0.539	1.08	0.979	0.979	1.49	1.07
THICKNESSES (in.):										
skin thickness, t1	0.1713	.1504	.0887	.0680	.0831	.0779	.0887	.0887	.0588	.0640
attched flange, t2	0.0726	.3089	.1503	.0905	.0644	.0891	.0568	.0568	.0780	.0903
web thickness, t3	0.0835	.0438	.0424	.0682	.0542	.0759	.0604	.0604	.0589	.0502
outstndng flnge,t4	0.0680	.0634	.0740	.0521	.0746	.0754	.0835	.0835	.1255	.0578
PART 3: LOCAL BUCKLING LOAD FACTOR OF THE OPTIMIZED DESIGN (PANDA2 prediction)										
	1.105	1.095	1.117	0.364	0.639	0.389	0.614	0.614	0.299	0.567
PART 4: LOCAL BUCKLING LOAD FACTOR OF THE OPTIMIZED DESIGN (BOSOR4 prediction)										
	1.114	1.119	1.131							
PART 5: LOCAL BUCKLING LOAD FACTOR OF THE OPTIMIZED DESIGN (STAGS prediction)										
	1.142	1.130	1.104	0.372	0.642	0.467	0.728	0.745	0.356	0.664
PART 6: WIDE COLUMN BUCKLING LOAD FACTOR (PANDA2 prediction)										
	1.116	1.143	1.134	1.147	1.088	1.310	1.277	1.282	1.145	2.110
PART 7: WIDE COLUMN BUCKLING LOAD FACTOR (BOSOR4 prediction)										
	1.125	1.161	1.185							
PART 8: LATERAL-TORSIONAL BUCKLING LOAD FACTOR (PANDA2 prediction)										
	1.100	1.134	1.385	1.067	1.099	1.053	1.048	1.048	1.090	1.095
PART 9: COLLAPSE LOAD FACTOR (STAGS prediction)										
	2.30	1.72	1.62	1.25	1.35	1.39	1.32	1.42	>1.7	1.72
PART 10: LOAD FACTOR FOR CRITICAL EFFECTIVE STRESS (PANDA2 prediction)										
	4.61	4.43	3.25	1.016	1.262	0.964	1.069	1.069	0.996	0.994
PART 11: LOAD FACTOR FOR CRITICAL EFFECTIVE STRESS (STAGS prediction)										
				0.91	1.1	1.15	1.20	1.20	1.05	1.07
PART 12: VALUES OF MARGINS AT THE OPTIMUM DESIGN ACCORDING TO PANDA2										
Column number------->	1	2	3	4	5	6	7	8	9	10
local buckling	0.005	-.001	-.016	----	----	----	----	----	----	----
bendng-tors buckl.	0.016	0.039	0.034	-.001	0.261	0.020	0.011	0.011	----	-.006
effective stress	3.61	3.43	2.250	0.016	0.262	-.036	0.069	0.069	-.004	-.006
mode jumping	0.675	0.729	0.593	----	-.002	----	-.028	-.028	0.482	0.627
wide column buckl.	0.060	0.144	0.082	0.043	-.011	0.191	0.161	0.165	0.041	0.920
laterl-tors buckl.	0.000	0.031	0.259	-.030	-.001	-.043	-.047	-.047	-.009	-.005
stringer seg. 2	24.3	190.0	60.7	11.6	8.70	11.2	5.86	5.86	----	----
stringer seg. 3	5.32	-0.002	-.003	0.402	-.001	0.665	0.290	0.290	0.169	0.238
stringer seg. 4	0.876	2.40	5.65	0.067	3.54	-.030	0.497	0.497	1.07	0.630
stringer seg. 3+4	1.37	-0.003	0.217	-.002	-.002	-.028	-.019	-.019	-.007	-.007
general buckling	0.026	-.001	-.001	0.150	0.103	0.369	0.381	0.427	0.843	1.50
stringer rolling	7.61	0.870	0.431	1.55	0.288	0.947	0.621	0.621	0.738	0.008
hiwave str rolling	1.39	1.27	2.33	0.554	1.46	0.159	0.340	0.340	0.213	0.452
str. web buckling	5.31	-0.002	-.003	0.462	0.041	0.408	0.072	0.072	0.034	-.010

Table 4 Comparison of predictions from PANDA2 and STAGS for the maximum effective stresses in various panels optimized by PANDA2 and loaded well into their local postbuckling regimes. The panel is loaded by the design load, axial resultant, Nx = -2000 lb/in.

Location in single module cross section	Max. Effective Stress (psi) from PANDA2	from STAGS	Figure in [58]
PART 1: Perfect "Z" panel optimized with the modejump constraint turned OFF (4)*			
At x=25 in. midway between stringers **	26391.	35200.	90
At x=25 in. in panel skin at rivet line	44204.	33500.	91
At x=29.75 in. in panel skin at rivet line	44204.	40000.	92
At x=25 in. in attached flange at rivet	35322.	33000.	93
At x=25 in. in attached flange next to web	37458.	36500.	94
At x=25 in. in web at web root	39073.	39000.	95
PART 2: Perfect "Z" panel optimized with the modejump constraint turned ON (5)			
At x=27.25 in. midway between stringers	26385.	35000.	113
At x=22.25 in. in panel skin at rivet line	30164.	22300.	114
At x=22.25 in. in attached flange at rivet	28939.	not obtained	
At x=22.25 in. attached flange next to web	34982.	30500.	115
At x=22.25 in. in web at web root	35663.	30000.	116
PART 3: Imperfect "Z" panel optimized with the modejump constraint turned OFF(6)			
At x=26.25 in. midway between stringers	29668.	33000.	138
At x=25.75 in. in panel skin at rivet line	44788.	36000.	139
At x=25.75 in. in attached flange at rivet	40511.	25000.	140
At x=20.75 in. attached flange next to web	45450.	33000.	141
At x=20.75 in. in web at web root	46698.	32500.	142
PART 4: Imperfect "Z" panel optimized with the modejump constraint turned ON (7)			
At x=21.75 in. midway between stringers	28199.	33000.	159
At x=21.75 in. in panel skin at rivet line	33234.	21000.	160
At x=25.75 in. in panel skin at rivet line	33234.	26000.	161
At x=21.75 in. in attached flange at rivet	30869.	25000.	162
At x=25.75 in. in attached flange at rivet	30869.	20000.	163
At x=21.75 in. attached flange next to web	42092.	28000.	164
At x=25.75 in. attached flange next to web	42092.	24000.	165
At x=21.75 in. in web at web root	39033.	25000.	166
At x=25.75 in. in web at web root	39033.	24000.	167
PART 5: Imperfect "J" panel optimized with the modejump constraint turned ON (9)			
At x=23.75 in. in panel skin next to base	45627.	42000.	205
At x=20.75 in. in base next to panel skin	45788.	33000.	206
At x=21.75 in. in base at web root	34904.	30500.	207
At x=23.75 in. in web at web root	35776.	30000.	208
PART 6: Imperfect "T" panel optimized with the modejump constraint turned ON(10)			
At x=27.25 in. in skin midway betw. stiff.	28794.	40600.	228
At x=23.25 in. in panel skin next to base	45169.	43500.	229
At x=22.25 in. in base next to panel skin	44743.	32000.	230
At x=25.00 in. in base at web root	31335.	not shown	
At x=25.00 in. in web at web root	28521.	not shown	

NOTES: * (n), where n = column number in Table 3
** x=25 in. corresponds to the panel midlength.

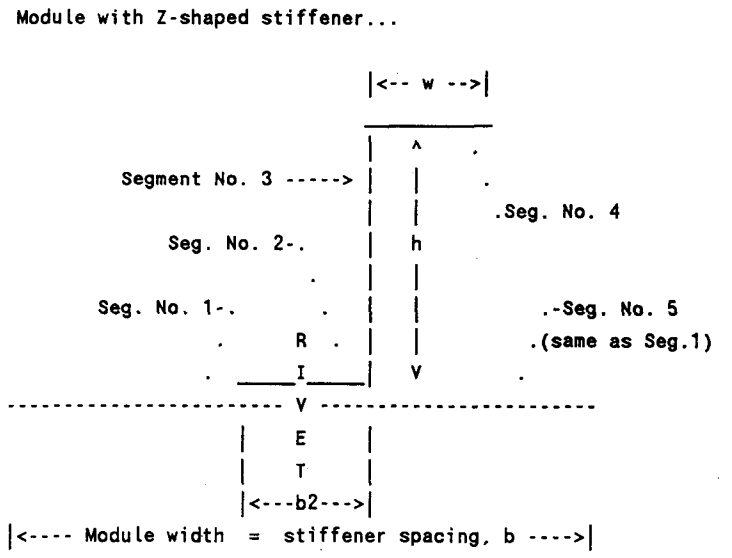

Fig. 1(a) Sketch of the Z-shaped stiffener in the PROMPT.DAT file

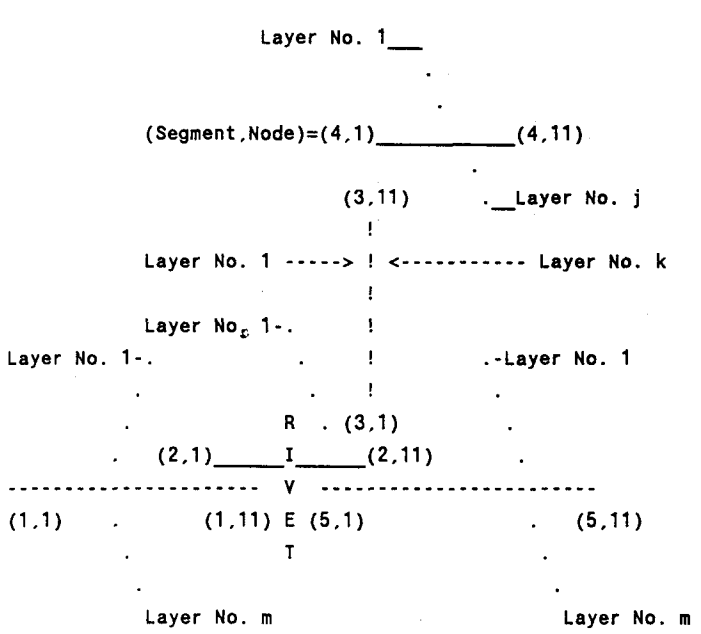

Fig. 1(b) Sketch of Z-shaped stiffener added to SUB. PICTS

The riveting of the faying flange to the panel skin is simulated by a junction constraint on displacements u,v,w, and rotation ROT at the midwidth of the faying flange (2,6) to the end node of Segment 1: (1,11). The heel of the Z-shaped stringer (intersection of Segment 2 with Segment 3) is free to lift off the panel skin. This renders the behavior of Z-shaped stringers considerably different from that of J-shaped stringers, especially for non-optimum designs.

FIG. 1

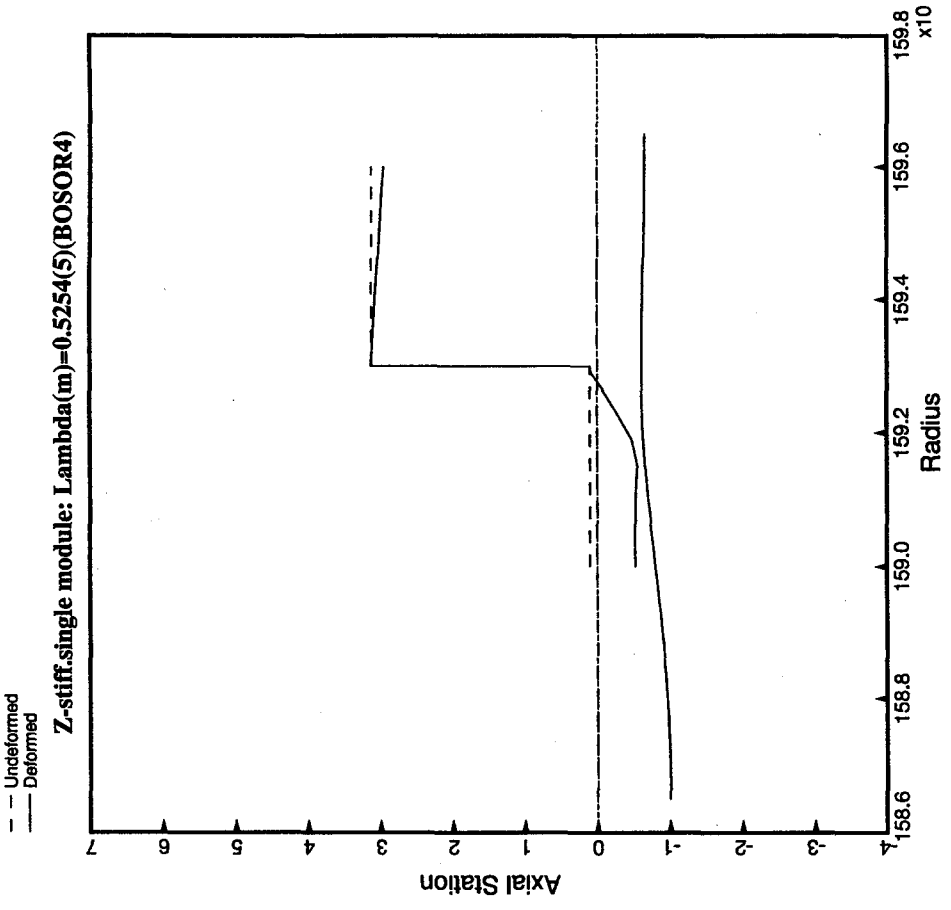

FIG. 3

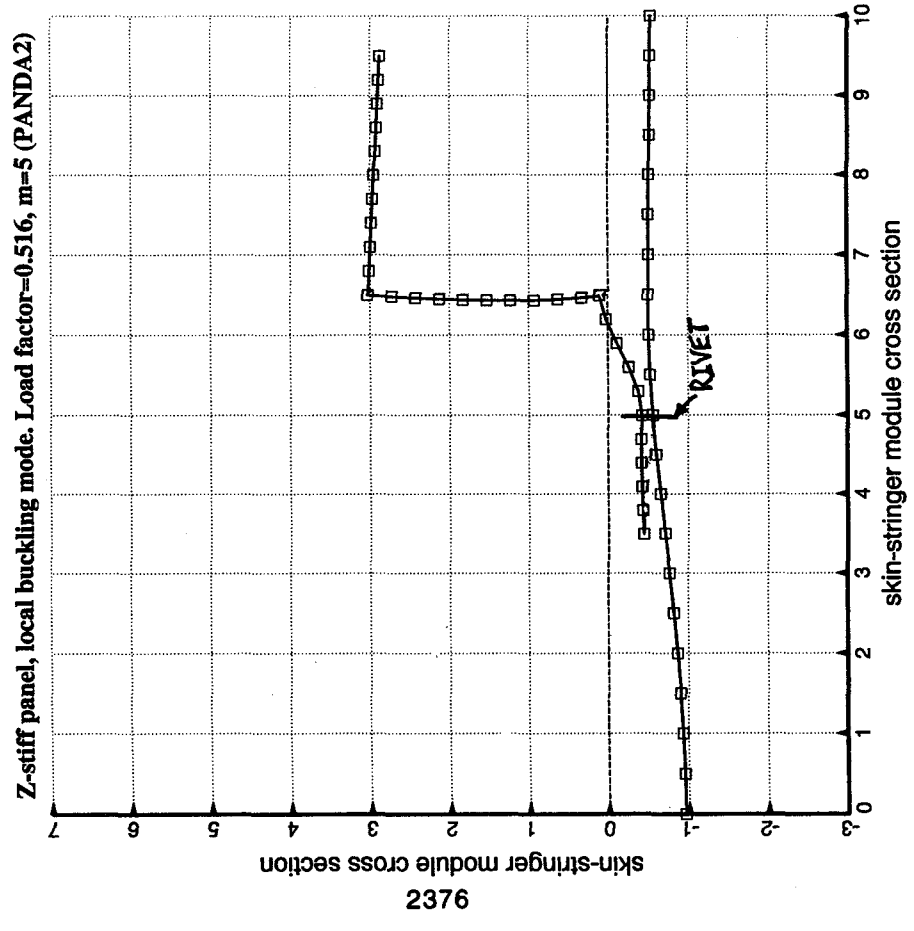

FIG. 2

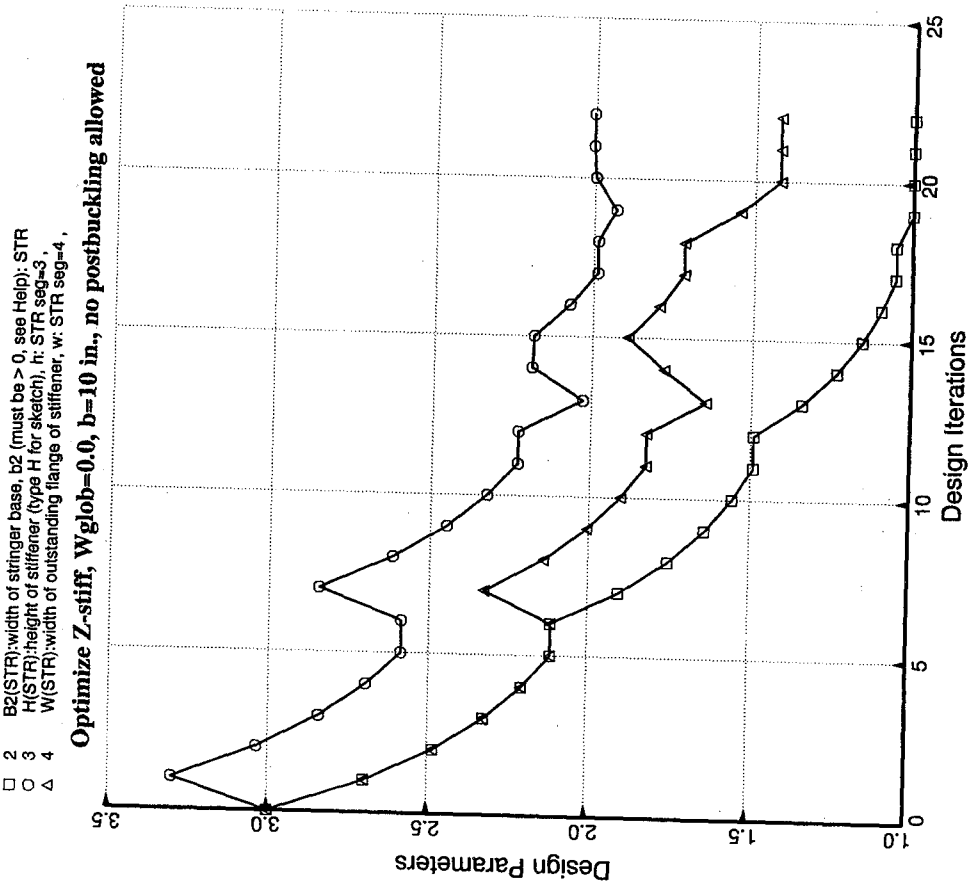

FIG. 5

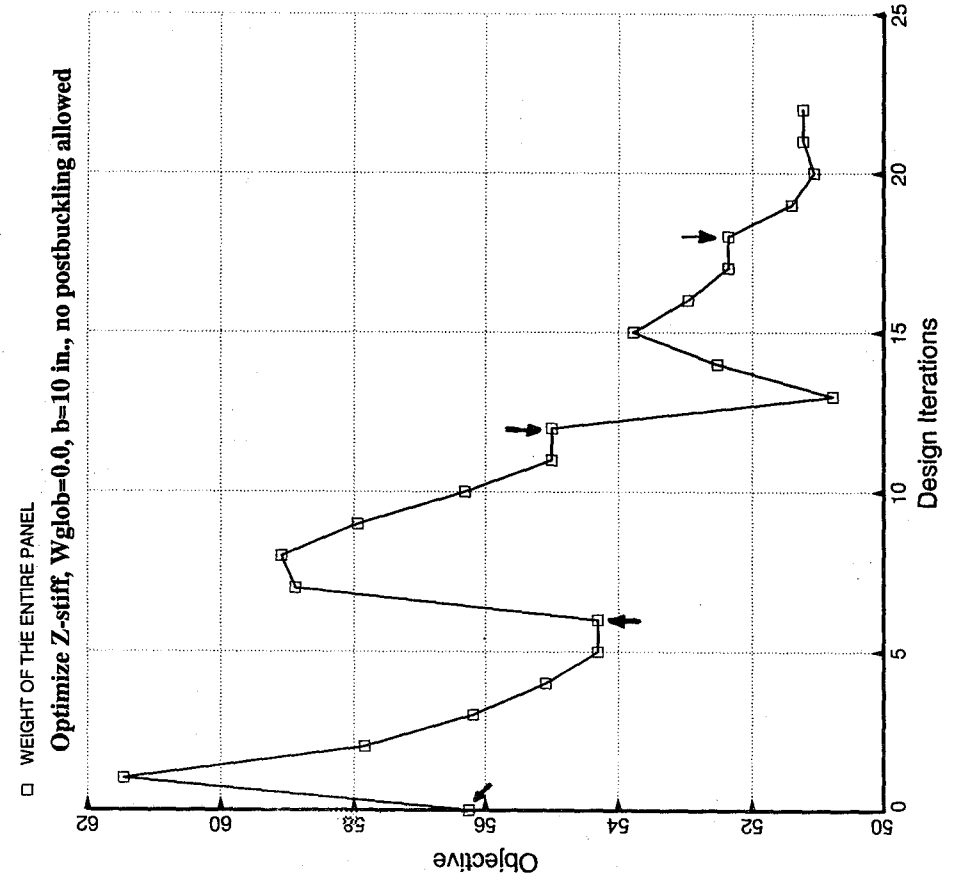

FIG. 4

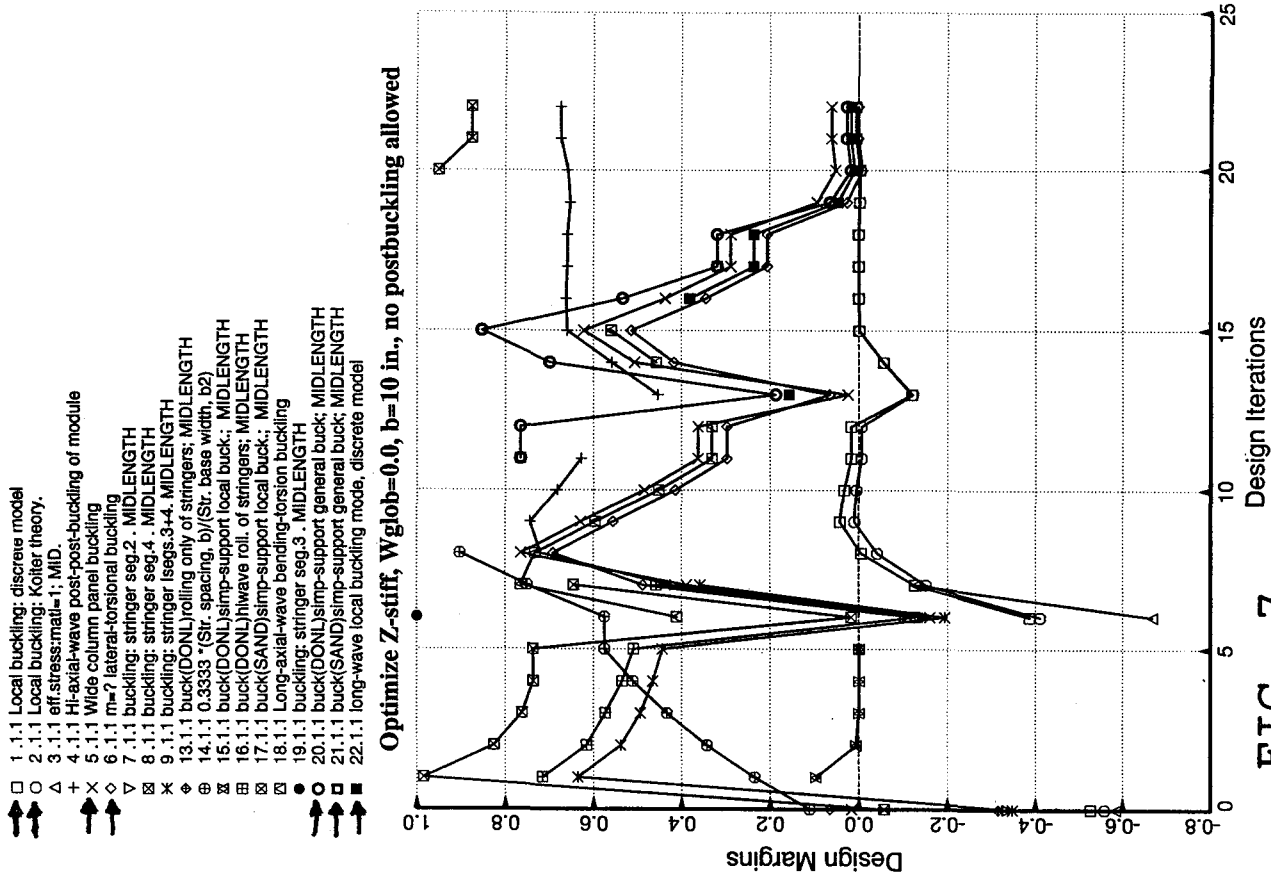

FIG. 7

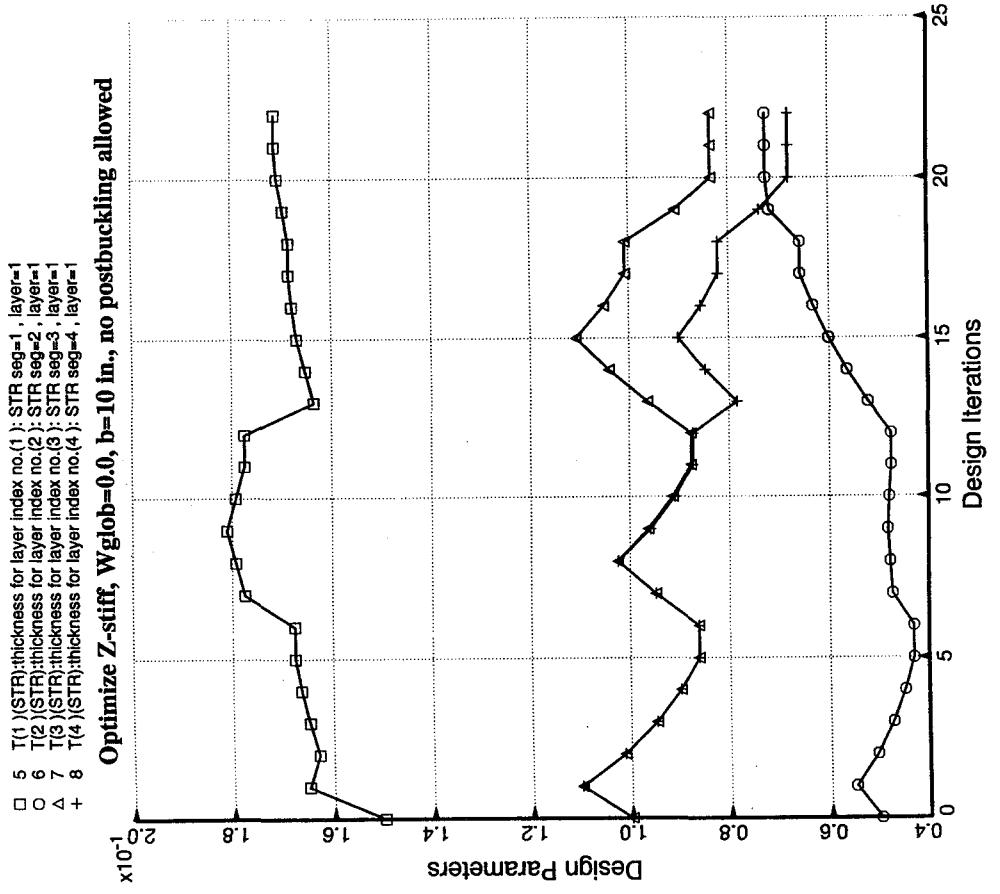

FIG. 6

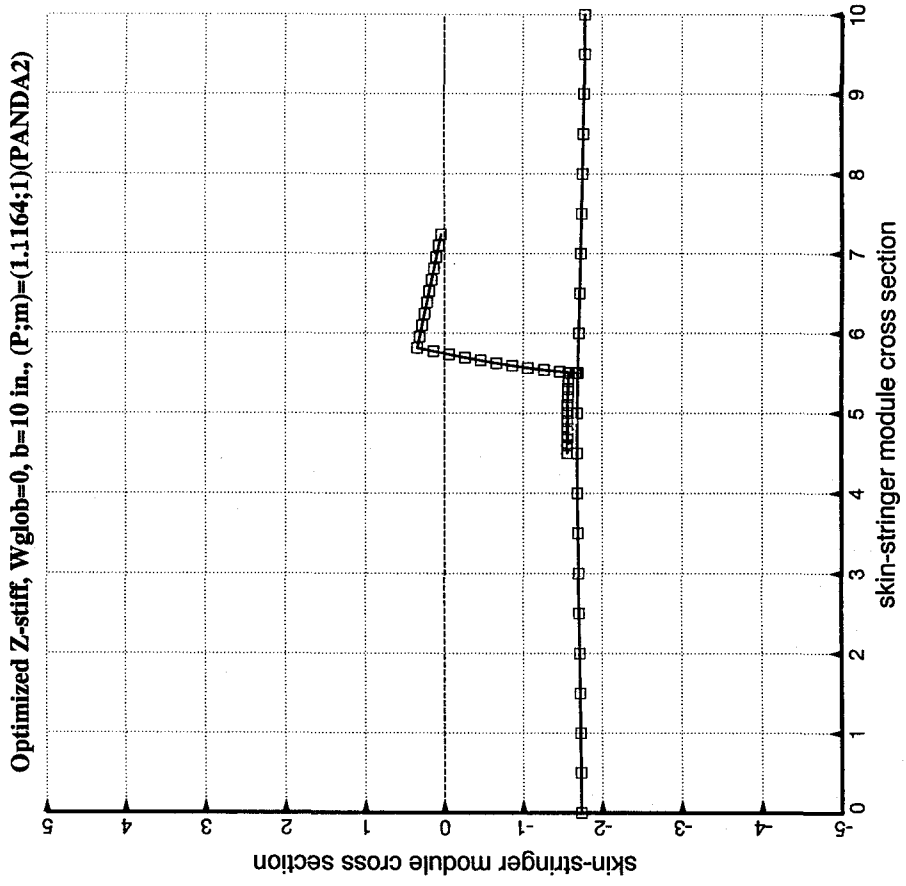

FIG. 9

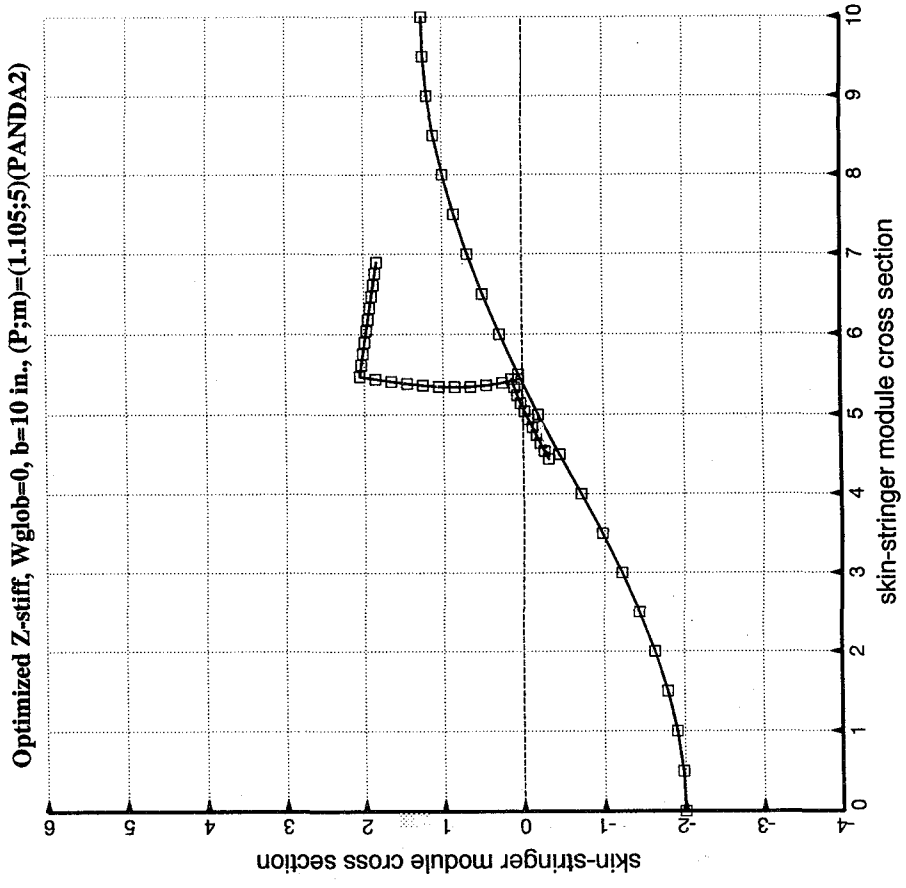

FIG. 8

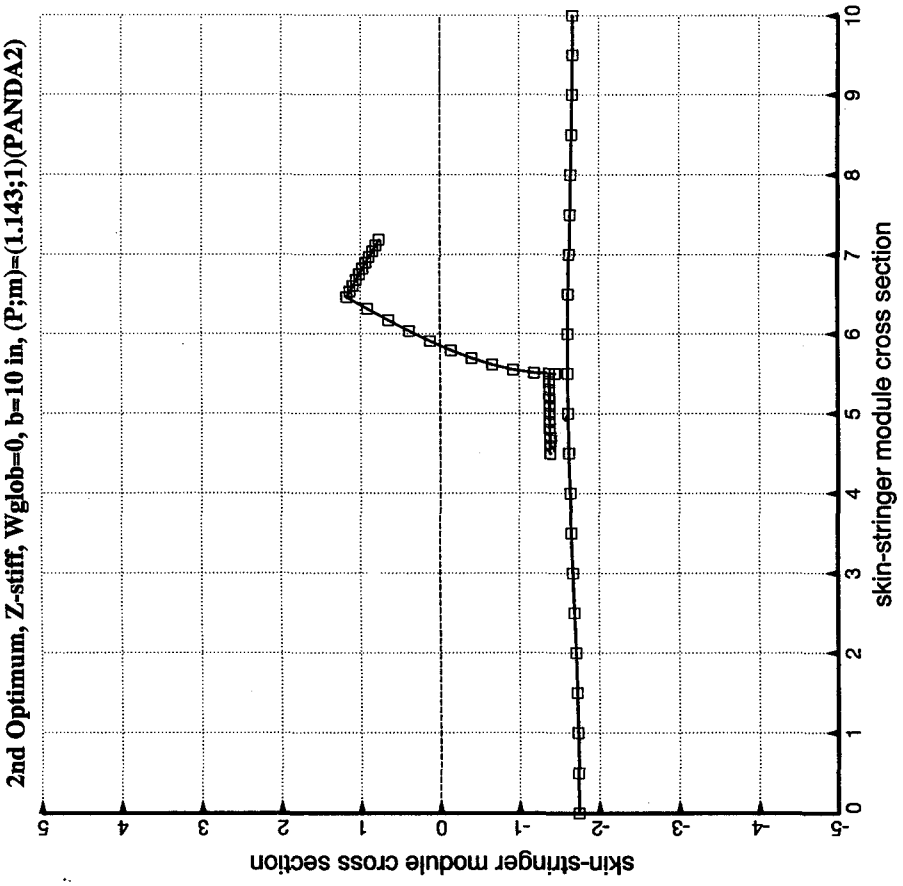

FIG. 11

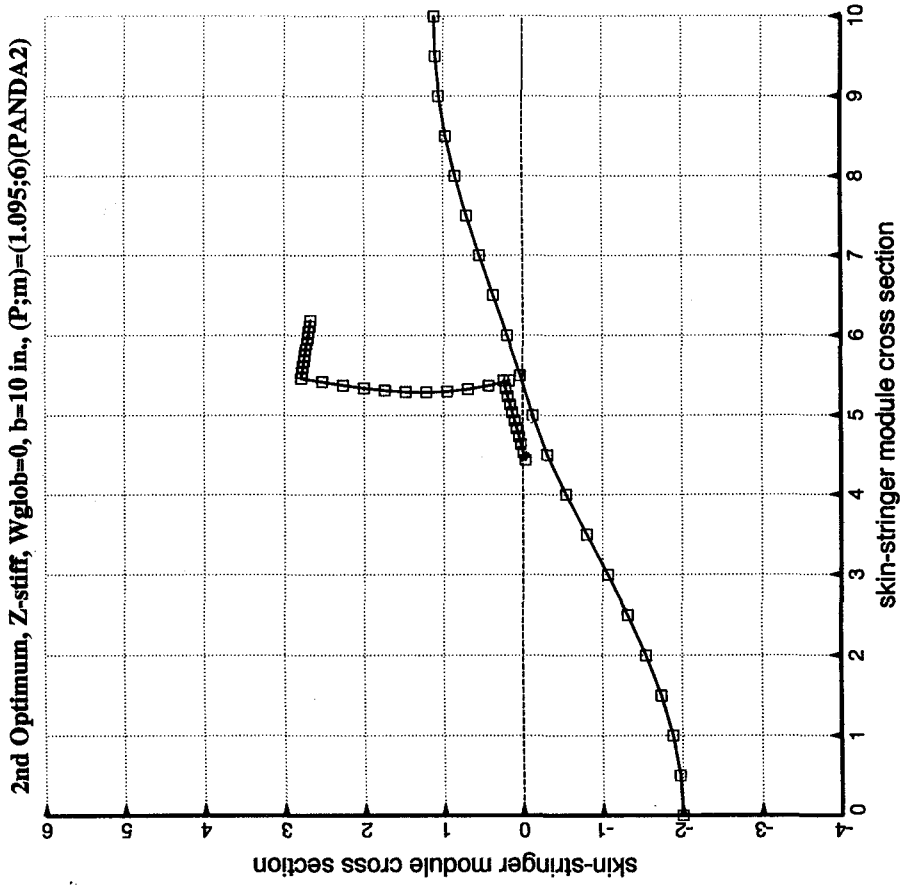

FIG. 10

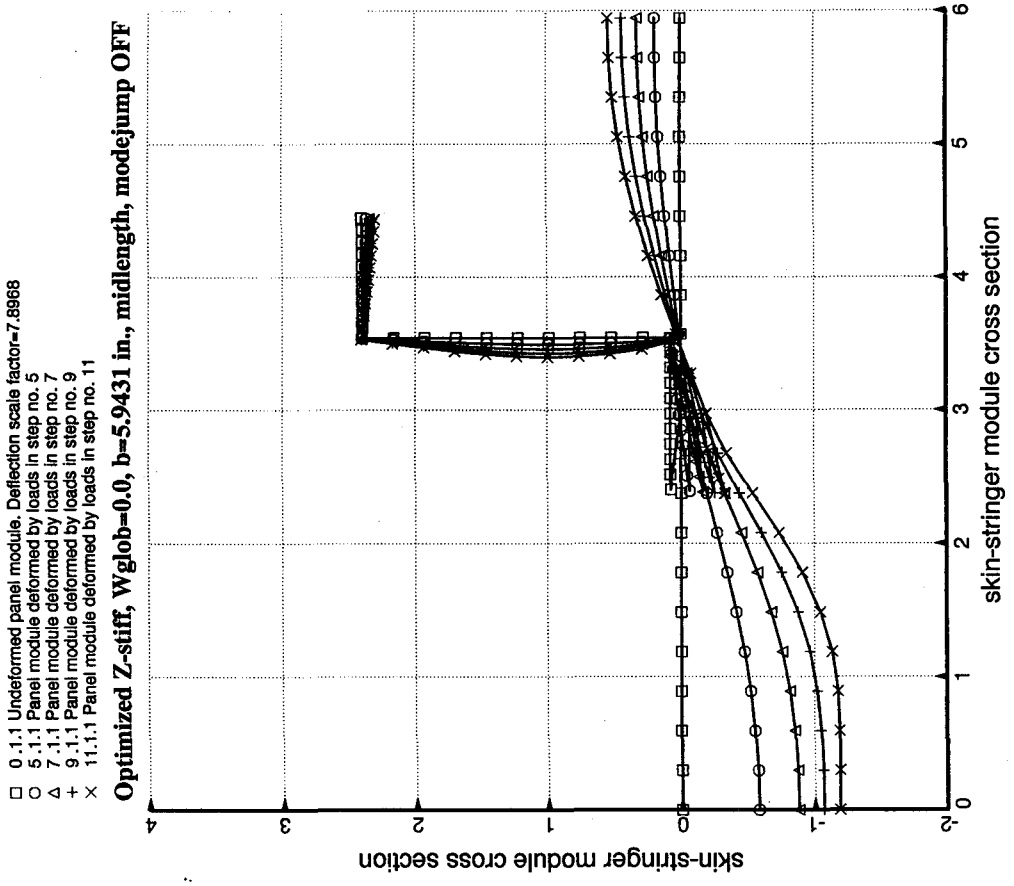

FIG. 13

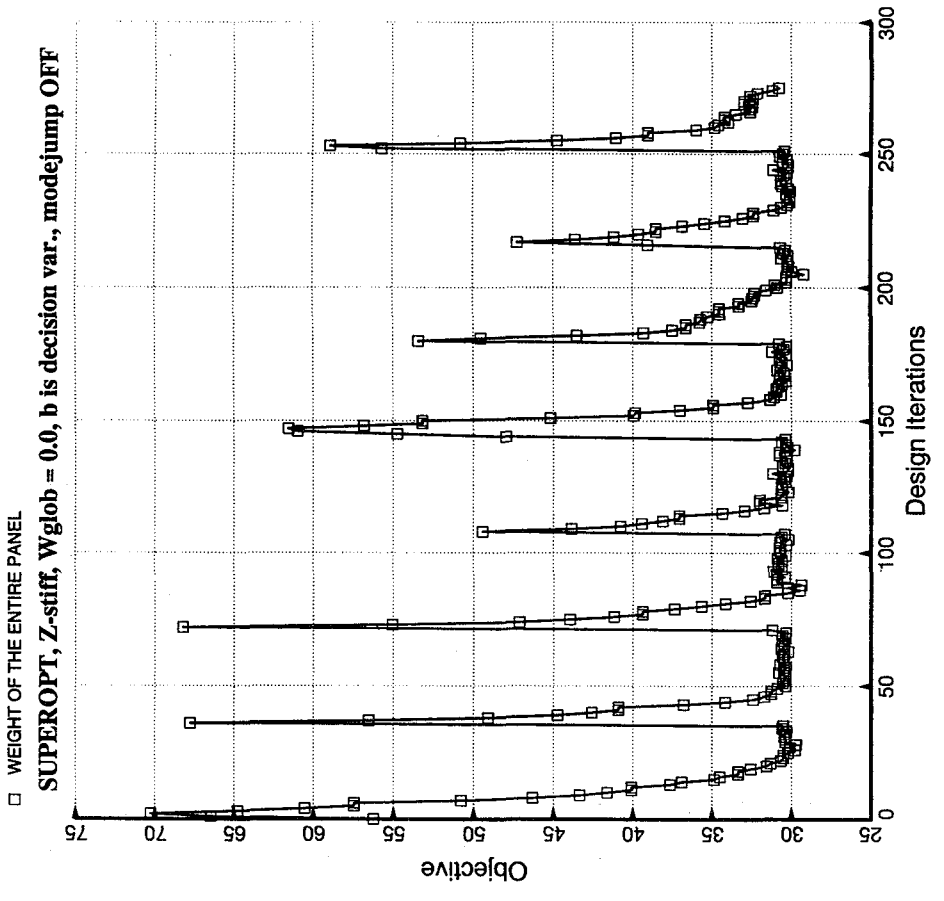

FIG. 12

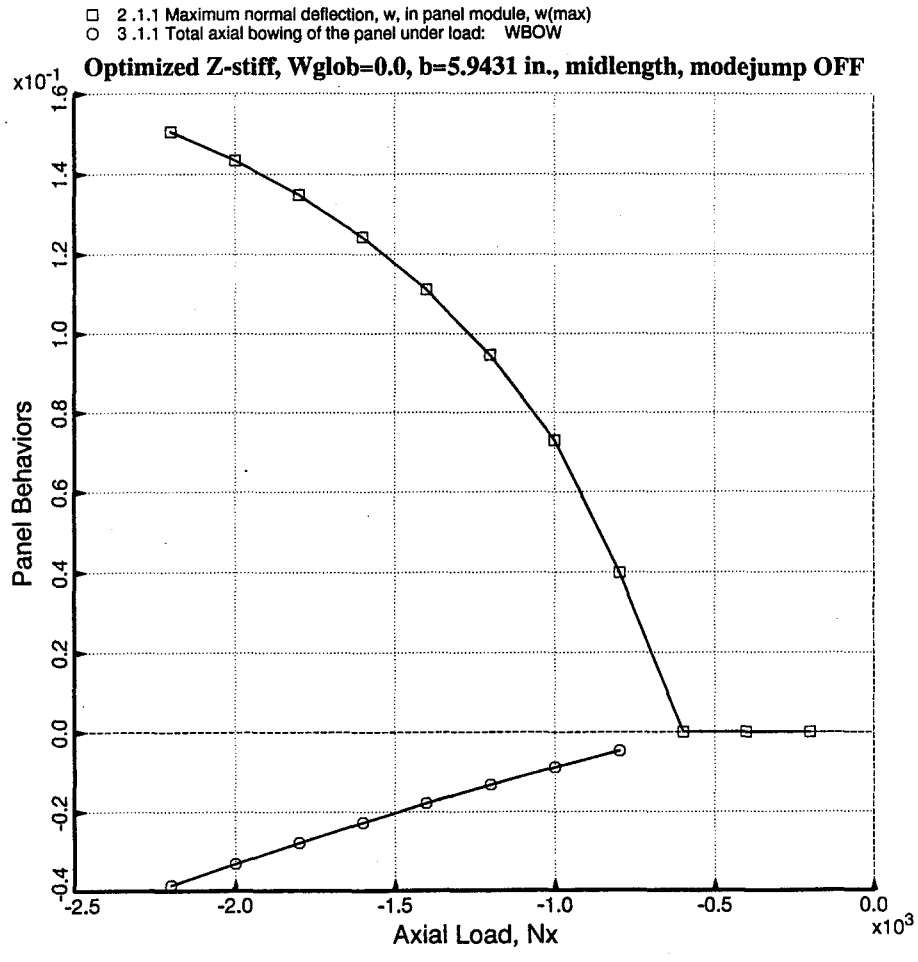

FIG. 14

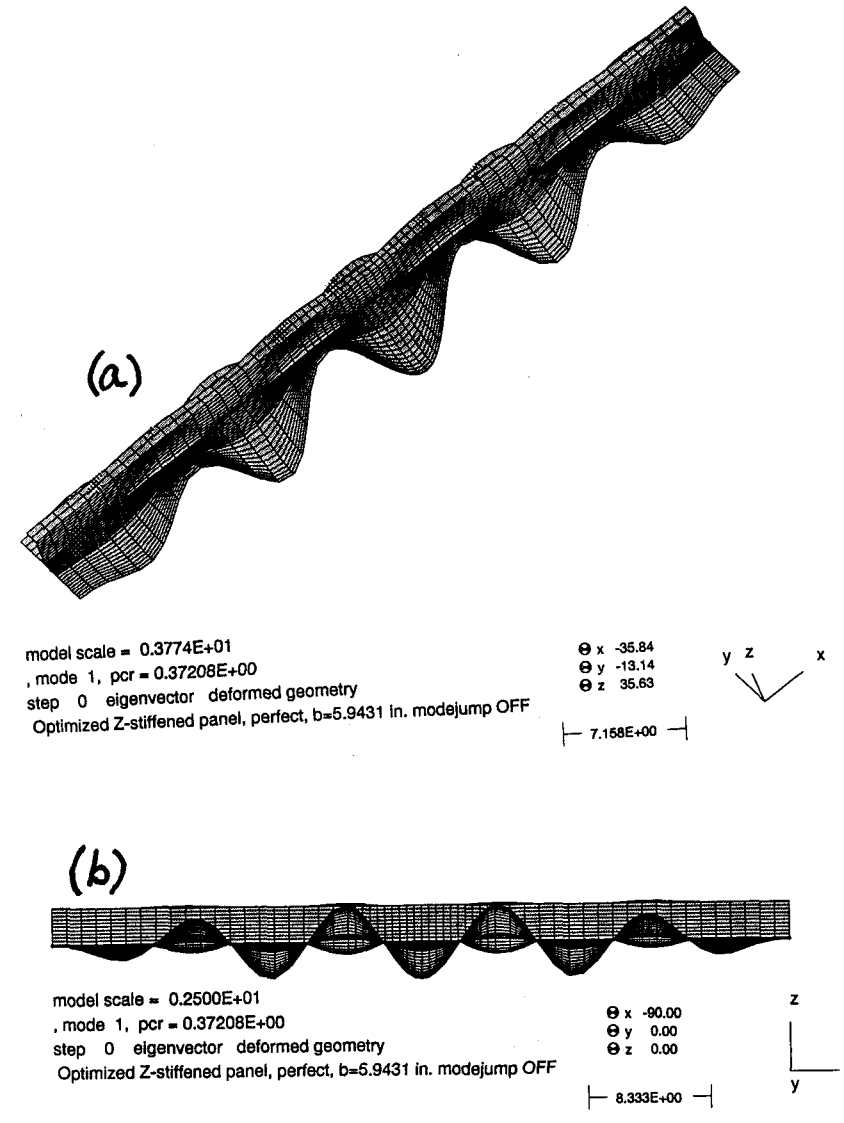

FIG. 15

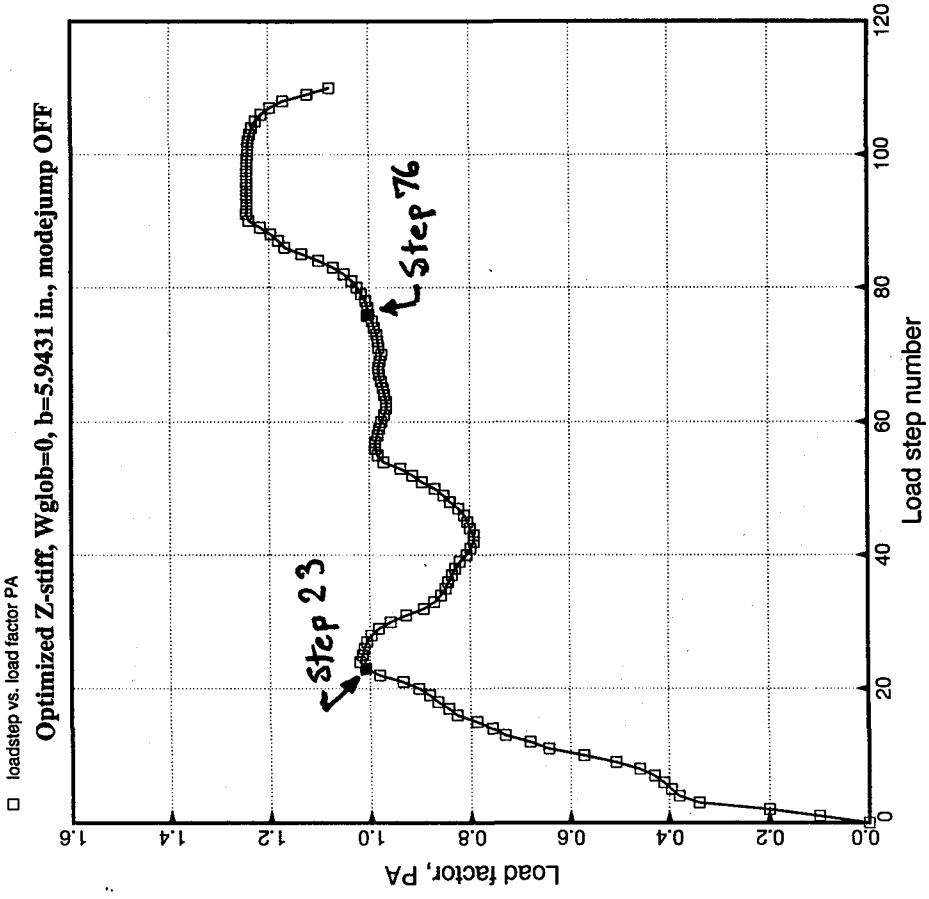

FIG. 17

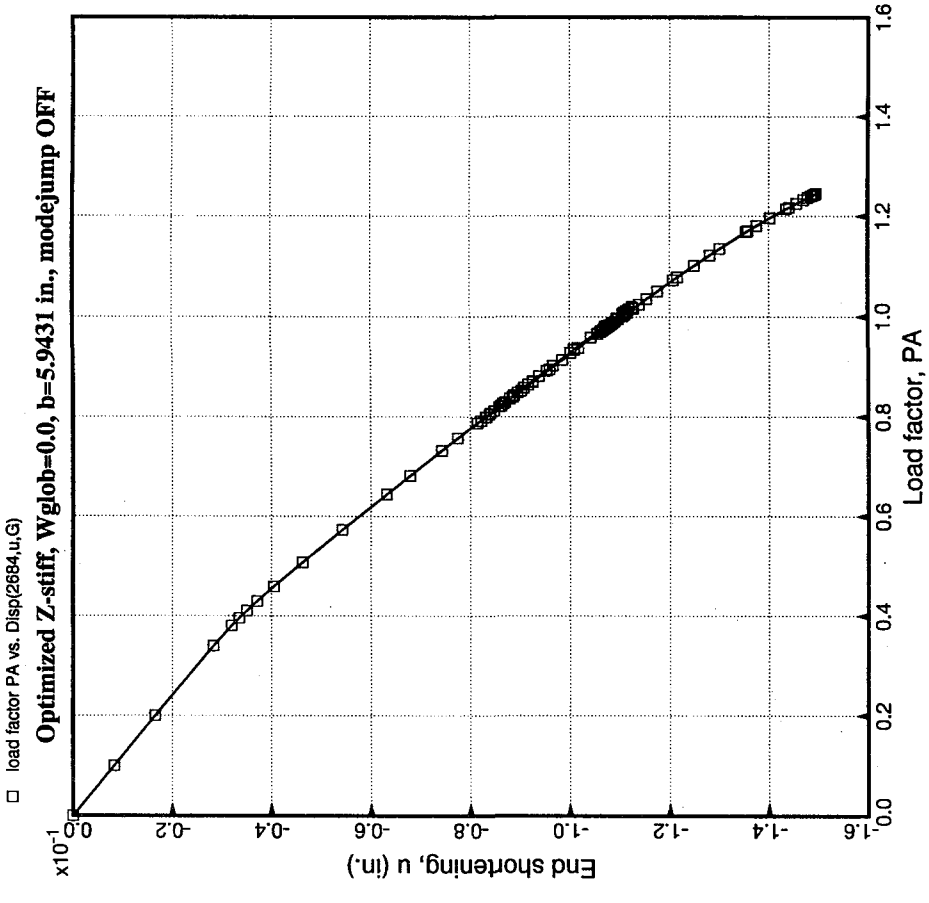

FIG. 16

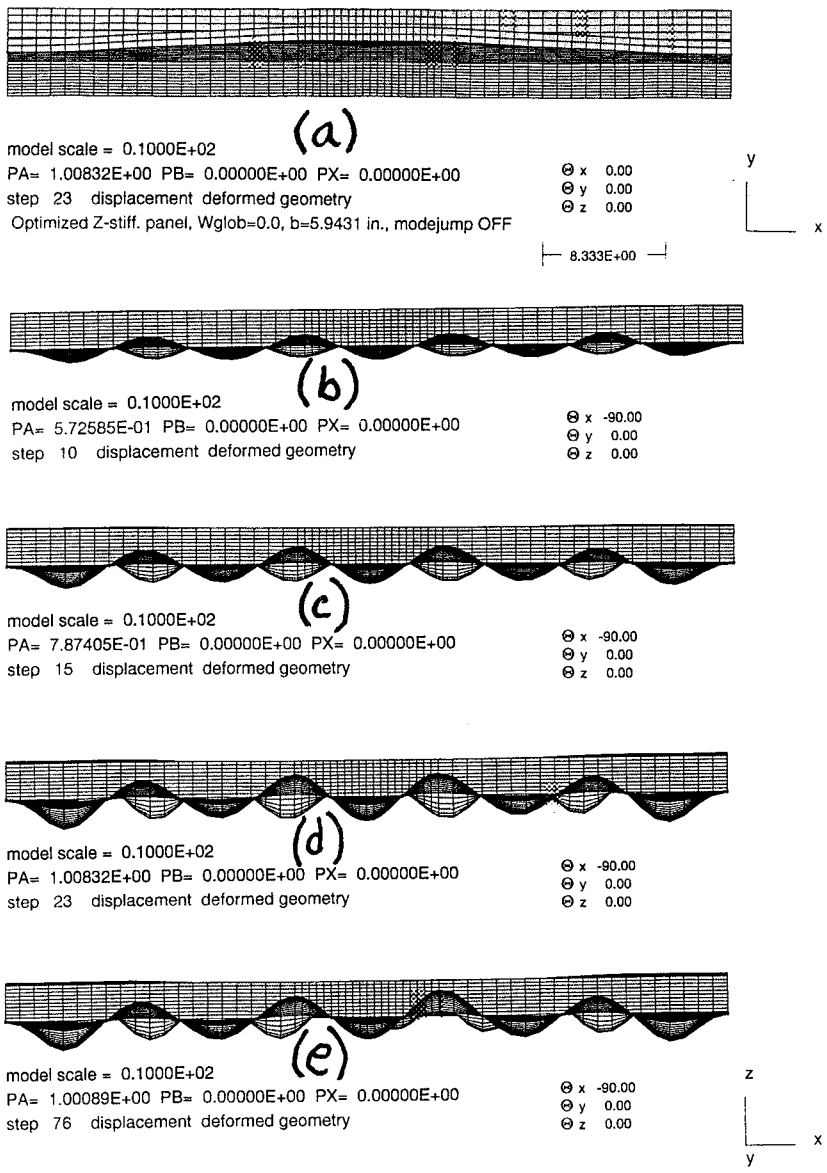

FIG. 18

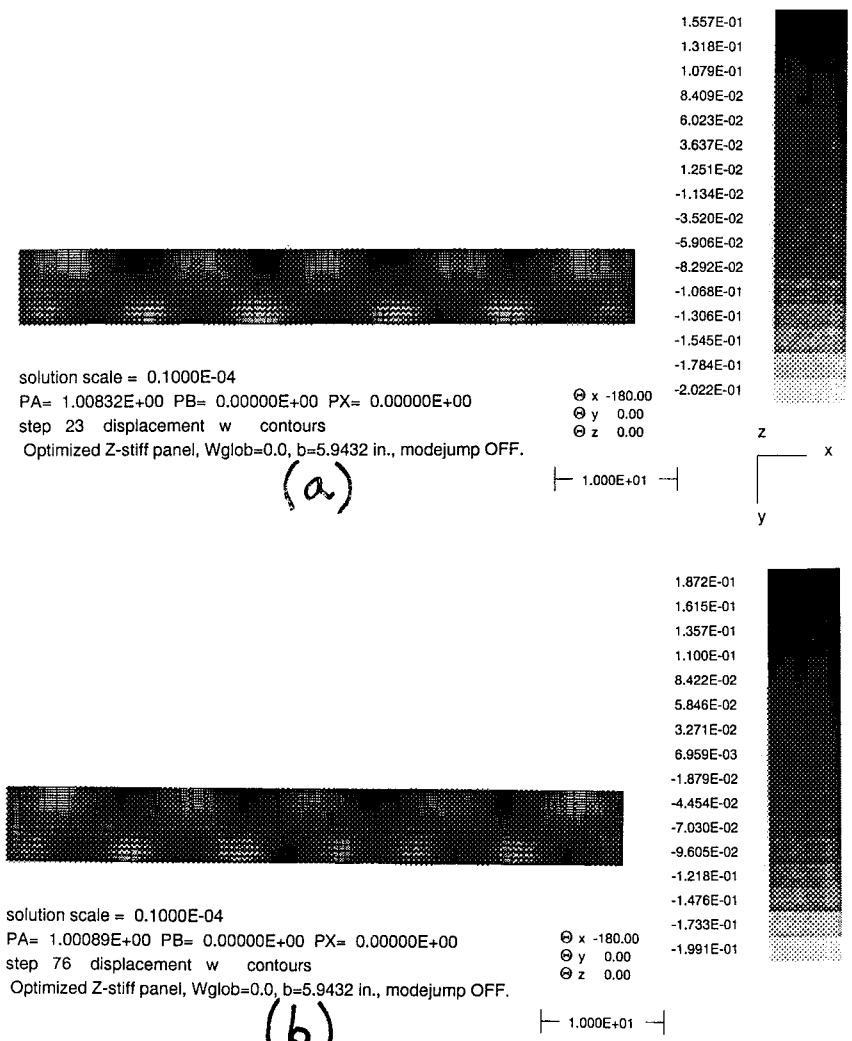

FIG. 19

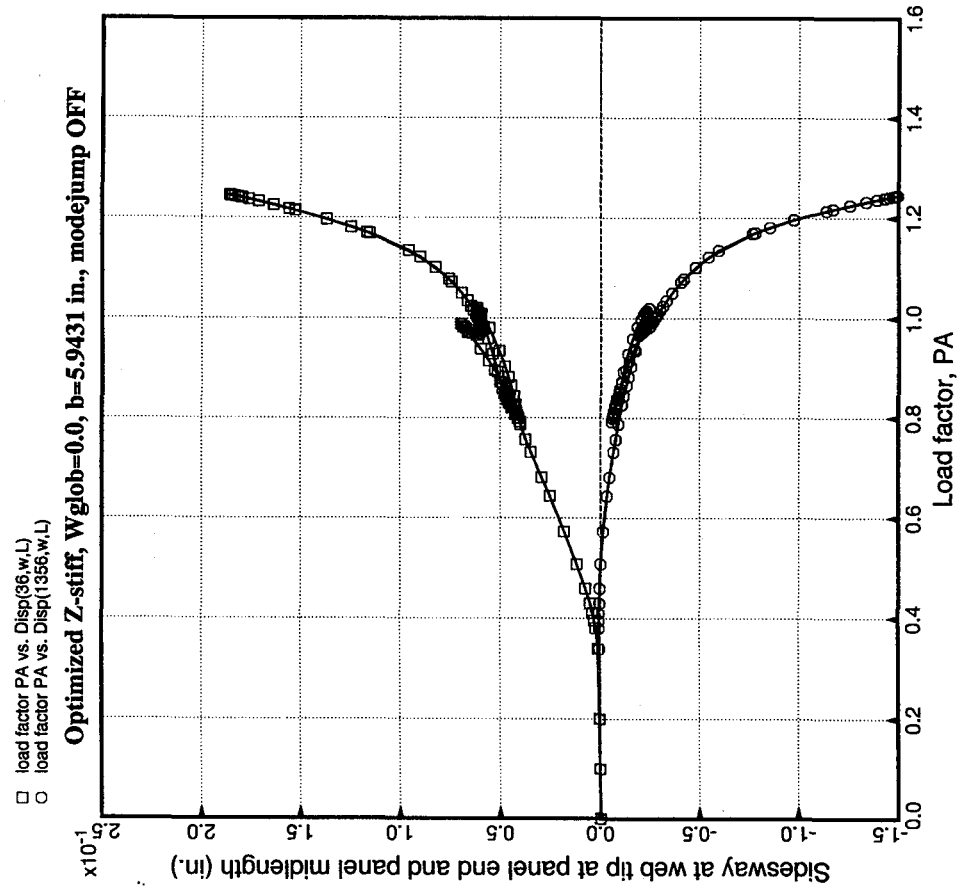

FIG. 21

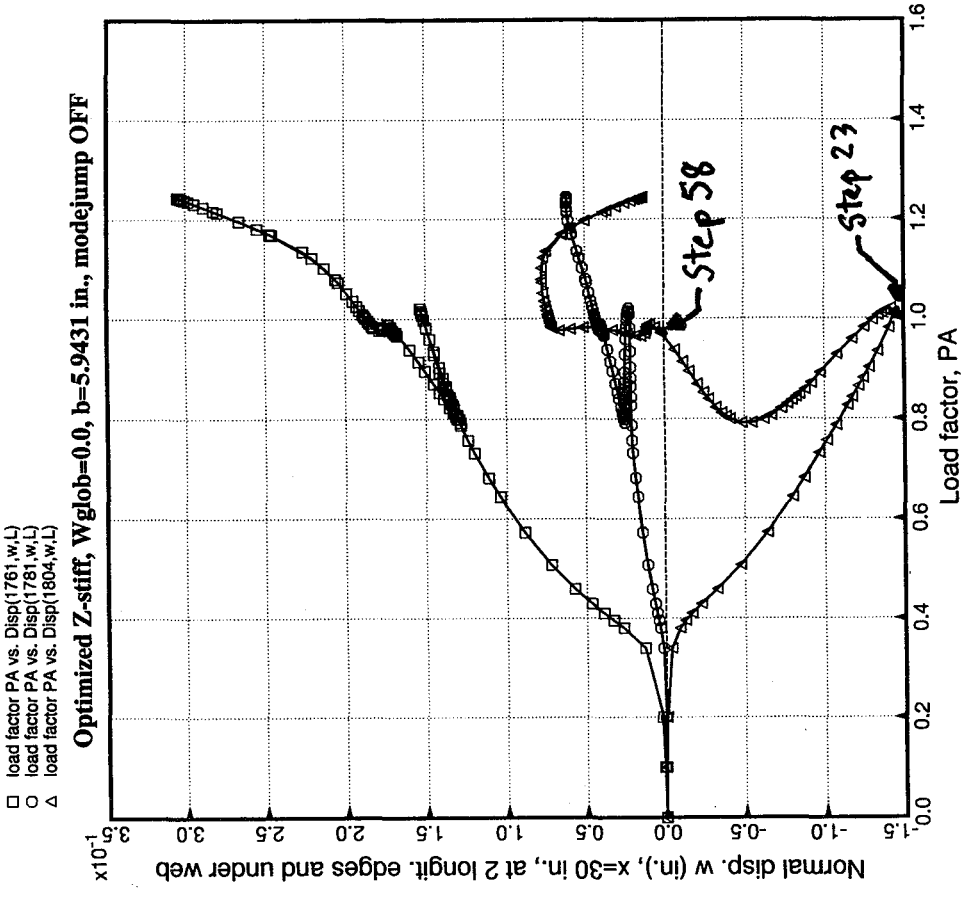

FIG. 20

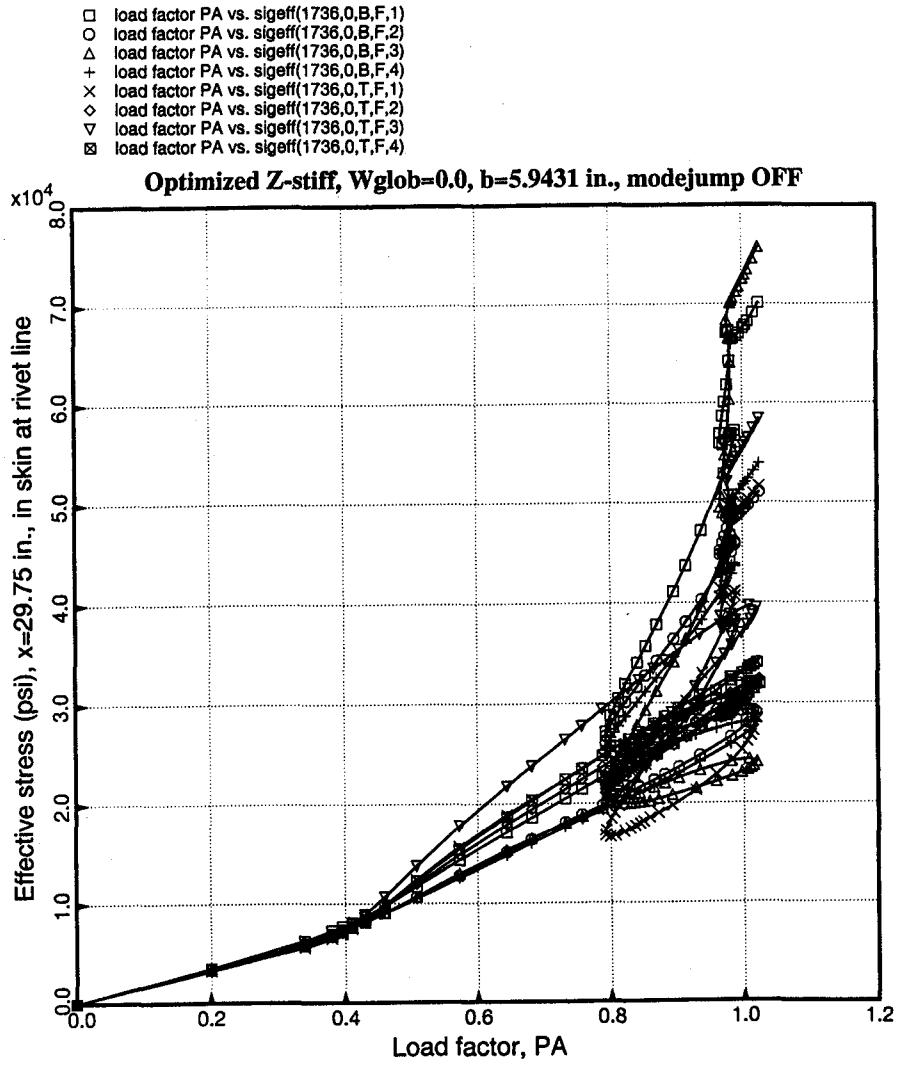

FIG. 22

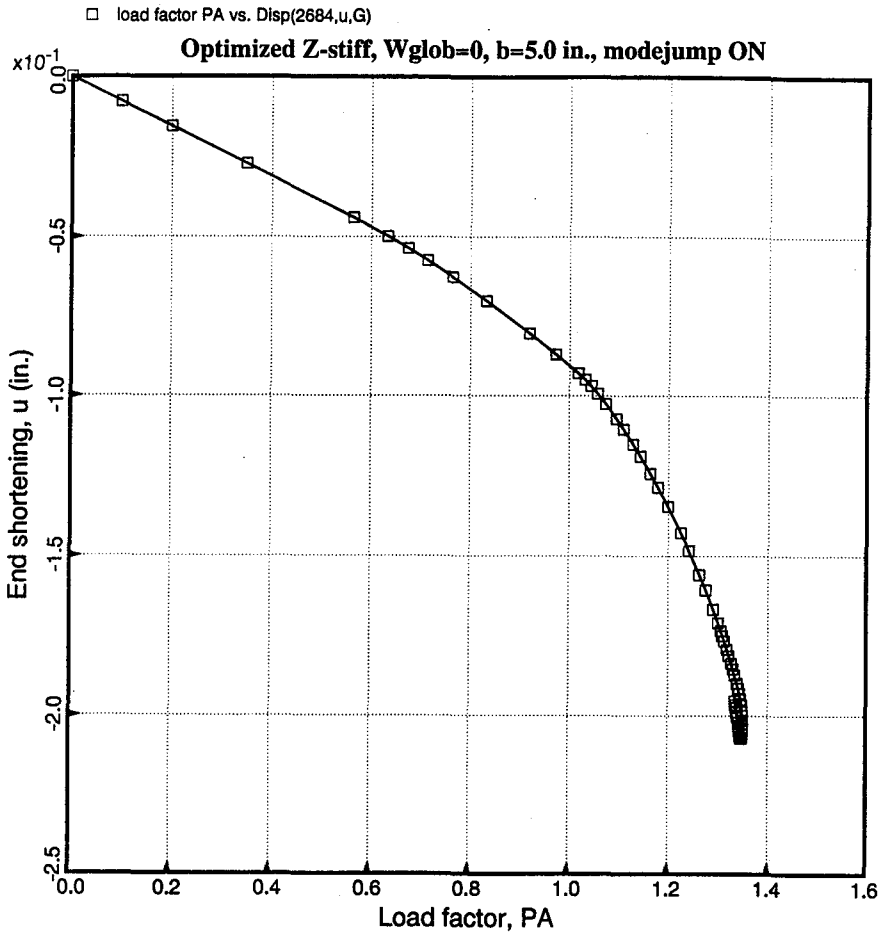

FIG. 23

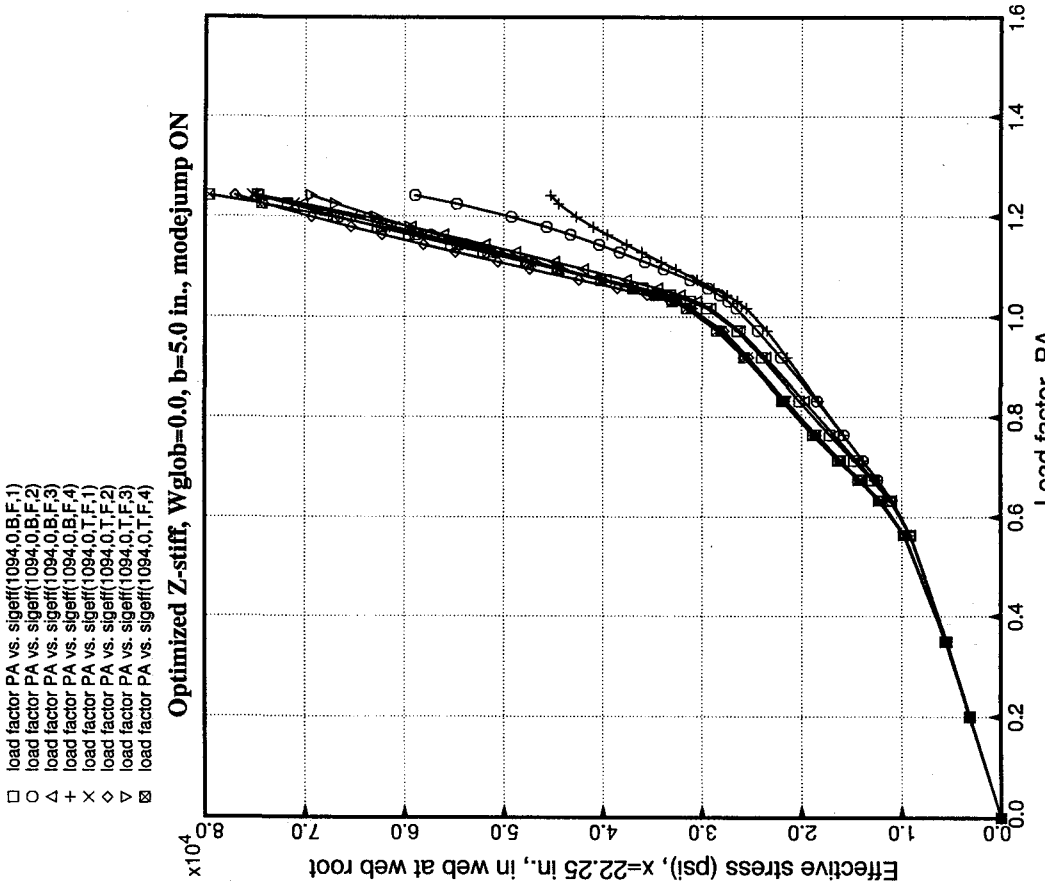

FIG. 25

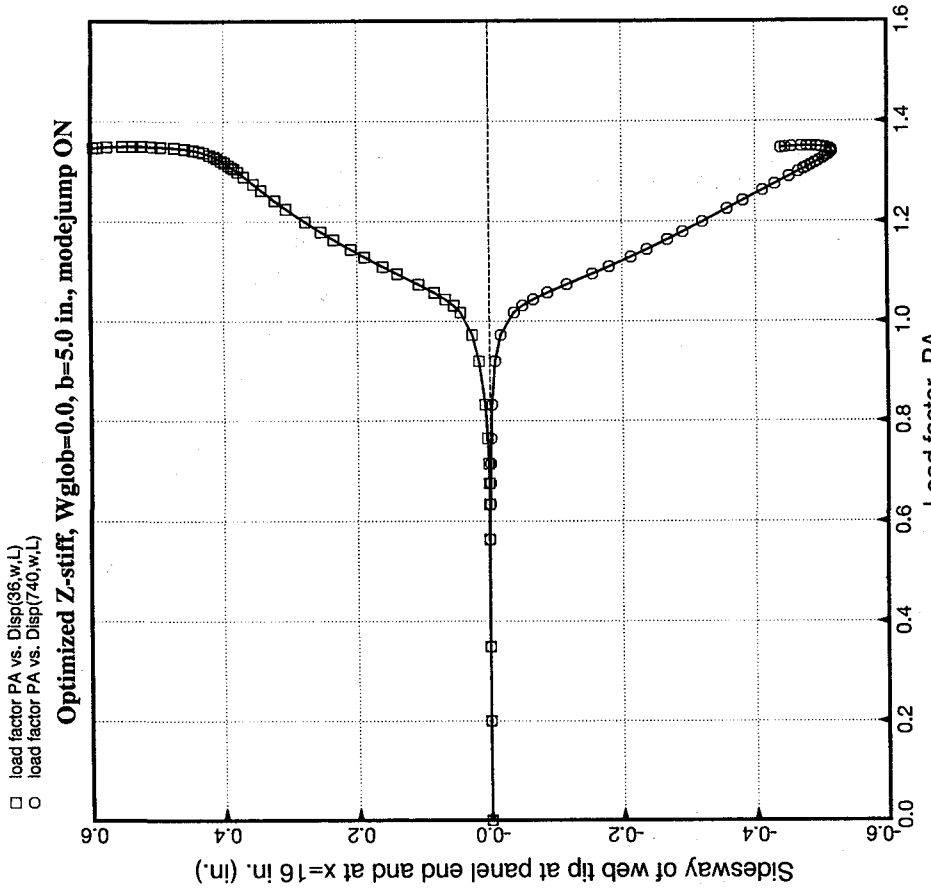

FIG. 24

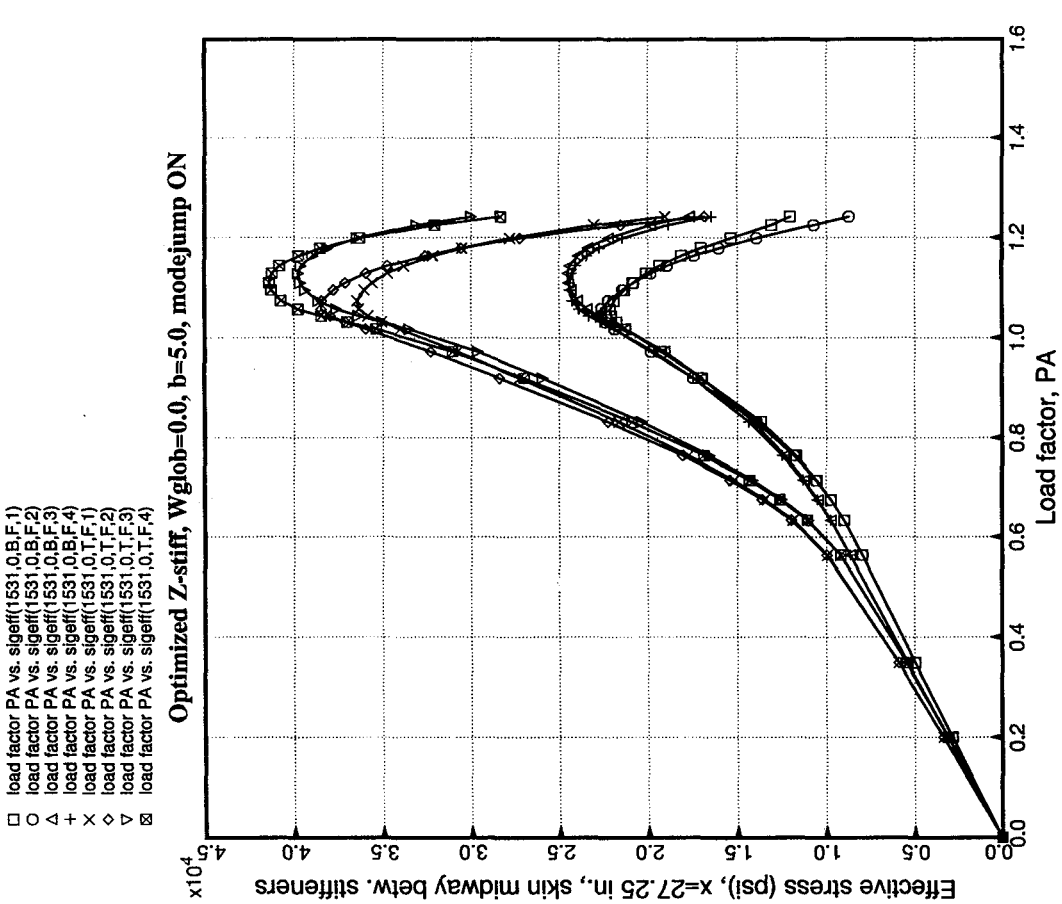

FIG. 27

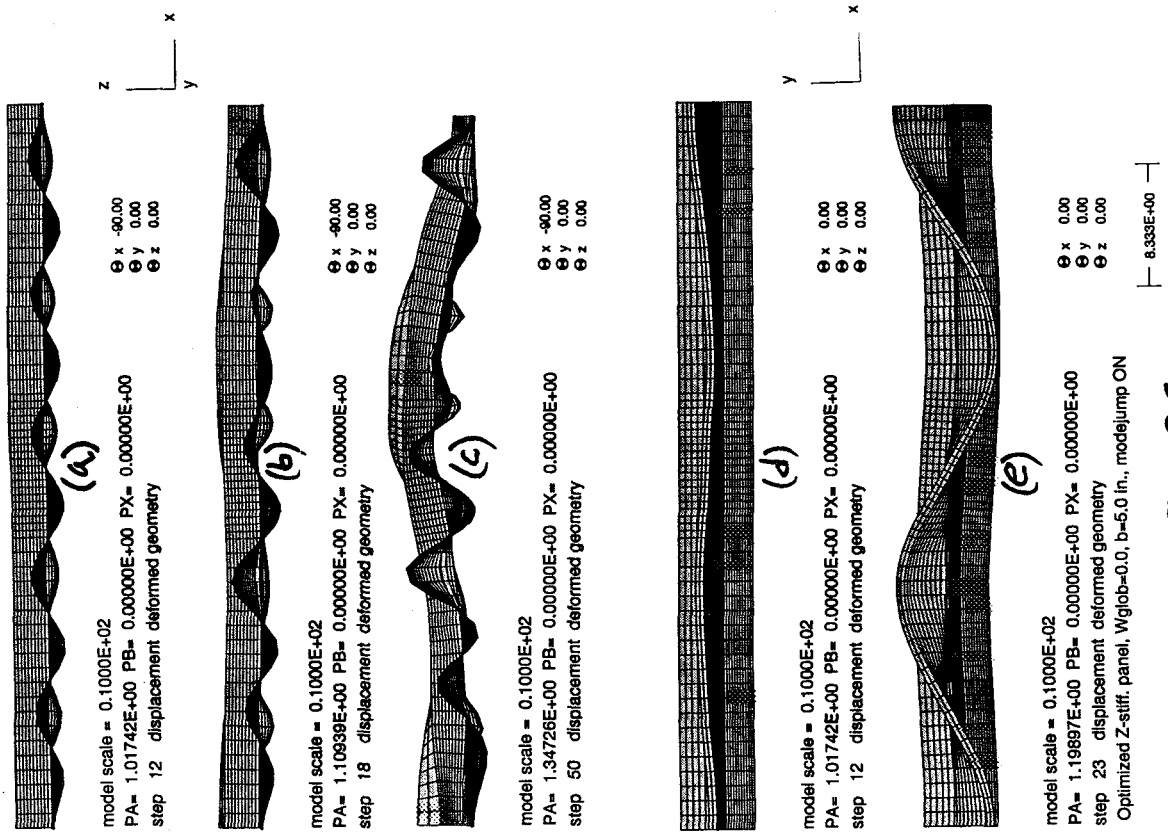

FIG. 26